Circadian patterns of energy metabolism are only partially reconstituted in gnotobiotic mice

Authors:

- Hoces, Daniel[1]
- Lan, Jiayi[2]
- Wenfei, Sun[3]
- Geiser, Tobias[1]
- Arnoldini, Markus[1]
- Nowok, Sven[4]
- Macpherson, Andrew J.[5]
- Stecher, Bärbel[6,7]
- Zenobi, Renato[2]
- Hardt, Wolf-Dietrich[8]
- Wolfrum, Christian[3]
- Slack, Emma[1,9]

1. Laboratory for Food Immunology, Institute of Food, Nutrition and Health, Department of Health Sciences and Technology, ETH Zürich, 8093 Zürich, Switzerland
2. Laboratory of Organic Chemistry, Department of Chemistry and Applied Biosciences, ETH Zürich, 8093 Zürich, Switzerland
3. Laboratory of Translational Nutrition Biology, Institute of Food, Nutrition and Health, Department of Health Sciences and Technology, ETH Zürich, 8603 Schwerzenbach, Switzerland
4. ETH Phenomics Center, Department of Biology, ETH Zürich, 8093 Zürich, Switzerland

5. Department of Biomedical Research, Gastroenterology & Mucosal Immunology, University of Bern, 3010 Bern, Switzerland
6. Max-von-Pettenkofer Institute, LMU Munich, Munich, Germany
7. German Center for Infection Research (DZIF), partner site LMU Munich, 80539 Munich, Germany
8. Institute of Microbiology, Department of Biology, ETH Zürich, 8093 Zürich, Switzerland
9. Corresponding author. Email: emma.slack@hest.ethz.ch

SUMMARY

Microbiota composition correlates with host metabolic health in both humans and mice. Here we investigated the extent to which a gnotobiotic microbiota can mimic the influence of a complete microbiota on mouse metabolism using an isolator-housed TSE-PhenoMaster® system. We found that energy expenditure was equivalent between germ-free (GF) and specific-opportunistic-pathogen free line (SPF) mice, and we extend this observation to the OligoMM12 microbiota (12 species across 5 phyla that are naturally abundant in a murine gut microbiota). Moreover, microbiota-released calories were well compensated by food intake in all groups. However, each group of mice have a distinctive circadian metabolic profile. OligoMM12 clustered with GF during the light phase, but with SPF during the dark phase for both RER and metabolome. Therefore, interactions between the host and a reductionist microbiota are non-uniform over the circadian cycle, revealing a promising tool to identify key microbiota species/functions that modify host metabolism.

KEYWORDS

Microbiota, Host Metabolism, Gnotobiotic.

INTRODUCTION

The gut microbiota is currently considered a key regulator of host energy metabolism (Sonnenburg and Bäckhed, 2016). In the absence of a microbiota, mice accumulated less fat (Bäckhed et al., 2004) and were protected from obesity induced by certain types of high-fat diets (Bäckhed et al., 2007; Fleissner et al., 2010; Kübeck et al., 2016). Several mechanisms have been proposed to explain this phenomenon and its relationship to metabolic imbalances (Cani et al., 2019). These include endocrine regulation of food intake (Goswami et al., 2018; Lin et al., 2012), additional energy liberated by the microbiota from dietary fibers (Turnbaugh et al., 2006), alterations in bile acid profiles (Sayin et al., 2013; Yao et al., 2018), inflammatory responses induced by some members of the microbiota (Caesar et al., 2015) and induction of thermogenesis in adipose tissue (Krisko et al., 2020; Li et al., 2019, 2021). However, given the complexity of a complete microbiota and its interactions with the host, validating any of these theories and identifying causal relationships remains a major experimental challenge (Harley and Karp, 2012; Walter et al., 2020).

Circadian variations in microbiota function adds an extra layer of complexity to metabolic interactions between the host and the microbiota. Circadian feeding is a major driver of microbiota composition (Thaiss et al., 2014; Zarrinpar et al., 2014). The luminal concentration of fermentation products such as short-chain fatty acids (SCFA) shows a dramatic circadian oscillation linked both to food intake and to intestinal motility (Tahara et al., 2018). Microbiota-derived molecules are known to influence host nutrient absorption (Wang et al., 2017) and host metabolic gene expression (Kuang et al., 2019; Thaiss et al., 2016). However, obtaining resolution on how these circadian variations affect host energy metabolism remains challenging and much of our current knowledge is derived from indirect calorimetry measurements made over a time period shorter than 24h (Bäckhed et al., 2004; Halatchev et al., 2019; Kübeck et al., 2016; Wostmann et al., 1968). Measurements of the same host-microbiota system, if taken at different timepoints in the circadian cycle of metabolism, could therefore be wrongly interpreted as qualitative shifts in

41 microbiota function. Consequently, to understand the influence of the microbiota on host energy
42 metabolism, it is key to register variation over the circadian cycle.

43 Gnotobiotic mice, colonized with a simplified microbiota made up of defined species, have become
44 a major tool to identify potential mechanisms of interaction between the microbiota and host (Koh
45 and Bäckhed, 2020; Mallapaty, 2017; Steimle et al., 2021). Simulations and mathematical analysis
46 can be applied with higher certainty to a defined consortium and the use of cultivable strains also
47 allows for *in vitro* analysis of metabolism and behavior of the strains. Such approaches can
48 generate a mechanistic understanding of how external factors (i.e. diet, infection) act on the
49 different microbiota members individually and at a community level (Faith et al., 2014; Kovatcheva-
50 Datchary et al., 2019). A widely used example, the OligoMM12, is a gnotobiotic consortium of 12
51 cultivable mouse-derived strains representing the major five bacterial phyla in the murine gut
52 (Brugiroux et al., 2016). It is reproducible between facilities (Eberl et al., 2020) and extensive data
53 now exists on the metabolism of individual species and their interactions with each other and the
54 host (Streidl et al., 2021; Weiss et al., 2021; Wotzka et al., 2019; Yilmaz et al., 2021). However,
55 working with these mice involves hygiene conditions similar to those required to work with germ-
56 free mice, which poses a technical challenge for the long-term analysis of mouse metabolism. In
57 particular, standard metabolic cage systems do not permit maintenance of an axenic environment
58 and moving mice between the isolator systems where such animals are normally bred to IVC-
59 cage-like systems can be associated with stress and behavioral abnormalities, which also
60 influence metabolism (Rabasa and Dickson, 2016). This explains why metabolic characterizations
61 of gnotobiotic mice are so scarce (Halatchev et al., 2019; Yao et al., 2018).

62 To address the challenge of long-term energy metabolism measurements in gnotobiotic mice, we
63 have built an isolator-housed metabolic cage system. Based on the TSE PhenoMaster® system,
64 we can monitor levels of O_2, CO_2 and hydrogen every 24min for up to 8 cages, across two separate

65 isolators, while maintaining a strict hygienic barrier. This way, longitudinal monitoring of
66 metabolism can be carried out over periods of several weeks in germ-free and gnotobiotic mice.

67 In this study, we explored how well a gnotobiotic microbiota replicates the influence of a complex
68 microbiota on host metabolism. We compared the metabolic profile of germ-free (GF), gnotobiotic
69 (OligoMM12) and conventionally raised mice (specific-opportunistic-pathogen free, SPF) fed *ad*
70 *libitum* with standard chow, using isolator-based indirect calorimetry. Similar to what has been
71 described before (Krisko et al., 2020; Kübeck et al., 2016), we found no significant differences in
72 energy expenditure among GF and SPF mice. These results are in contrast to other work
73 (Bäckhed et al., 2004; Levenson et al., 1969; Li et al., 2019; Wostmann et al., 1968), but the
74 discrepancies can potentially be explained by the methods applied for normalizing energy-
75 expenditure data. These methods consider (or not) that germ-free and gnotobiotic mice exhibit
76 extensive water retention in the cecal lumen which can contribute up to 10% of the total body
77 weight. When accounting for cecal inert mass, we also observed no significant difference in energy
78 expenditure in the gnotobiotic OligoMM12 mouse line (Brugiroux et al., 2016). Interestingly,
79 despite indistinguishable energy expenditure, and indistinguishable energy absorption from food
80 each day, OligoMM12 mice showed increased fat mass compared to both, germ-free and SPF
81 mice. Moreover, their circadian patterns of respiratory exchange ratio (RER) and certain
82 metabolites in liver and plasma, phenocopied SPF mice during the dark phase, but germ-free mice
83 during the light phase. Our study shows how a reductionist/synthetic microbiota can specifically
84 recover microbiota function in the dark (active) phase, but not in the light (resting/fasting) phase
85 of the circadian cycle. This represents a powerful tool for identifying critical microbiota species and
86 functions needed to support healthy host metabolism throughout the day.

87 **RESULTS**

88 To describe the influence of the microbiota on the metabolic profile of mice, and to be able to
89 compare to published literature, we compared male, adult age-matched (12-14wks old) germ-free
90 (GF), gnotobiotic (OligoMM12) and conventionally raised (SPF) mice, all bred and raised in
91 flexible-film isolators and with a C57BL/6J genetic background. As these data are inherently noisy,
92 and data quality can be improved considerably by pooling data of multiple days and animals, we
93 needed to carry out indirect calorimetry in a system where we could be certain that the risk of
94 microbial contamination is very close to zero. We therefore adapted flexible-film surgical isolators
95 to accommodate a TSE PhenoMaster® system (schematic view in Fig. 1A, picture Fig. 1B) to
96 perform indirect calorimetry measurements of eight single housed mice. Mice were adapted for
97 between 24-36h to the single-housing condition inside isolator-based metabolic chambers before
98 data collection. Variations on O_2, CO_2 and hydrogen, along with food and water consumption,
99 were recorded every 24 min on each metabolic cage.

100 **Body composition in GF, OligoMM12 and SPF mice**

101 After 6-12 days of data recording mice were fasted for 4-5 hours and euthanized (approximately
102 at ZT6 ± 1 hour), and body mass and body composition were measured. As cecal mass (cecal
103 tissue plus its content) is affected by the colonization status (Wostmann et al., 1968), we first
104 assessed the cecal mass in GF, OligoMM12 and SPF and its impact on body mass. We found
105 that cecal mass was inversely correlated to the microbiota complexity, starting at approximately
106 0.5 g in SPF mice, increasing to around 1.5 g in OligoMM12 mice and reaching 3 g on average in
107 GF mice (Fig.1C).

108 Given that the cecal mass represents a major proportion of total body mass, accounting for
109 approximately 10% in GF mice (Suppl. Fig.1A), we compared the body mass of GF, OligoMM12

110 and SPF mice before and after the removal of the cecal mass. Although we found no significant
111 difference between these mice, we observed a trend in total body mass with GF mice showing
112 higher mass than SPF and OligoMM12 mice (Fig, 1D). This trend was completely reverted after
113 removal of the cecum (Fig. 1E).

114 Measurements of body composition in mice are typically performed using EchoMRI, which yields
115 data on lean, fat and water mass. As we observed that the cecum represented such a large and
116 variable fraction of body mass, it was essential to compare EchoMRI read-outs of “lean” and “fat”
117 body mass before and after removal of the cecum (Suppl. Fig.1B-G). We found a strong correlation
118 between the total lean mass measured by EchoMRI with and without the cecum (Suppl. Fig 1B),
119 with a decrease on the lean mass readout by EchoMRI after cecum removal ranging from around
120 1.3 g in SPF mice up to approximately 2 g in GF mice (Suppl. Fig.1C), i.e., 5 to 10% of the original
121 lean mass readout (Suppl. Fig. 1D). We concluded that a relatively consistent mass of cecum
122 seems to be scored as lean mass by EchoMRI, regardless of total cecum size, and all groups of
123 mice are similarly affected. Therefore, for ease of comparison to published work, we decided to
124 report and to use lean mass obtained by EchoMRI *before dissection* for definitive energy
125 expenditure calculations. We observed a trend in lean body mass with GF having a lower lean
126 body mass than SPF mice, and OligoMM12 mice showing an intermediate phenotype (Fig. 1F).
127 However, we were underpowered to detect a significant difference between groups, and we
128 estimate that at least 22 mice per group would be needed to achieve statistical significance by
129 one-way ANOVA if the current group differences are real – a number that was beyond the scope
130 of the current study.

131 Interestingly, EchoMRI fat mass measurements pre- and post-cecum dissection were poorly
132 correlated in GF mice (Suppl. Fig. 1E) attributable to a rather variable scoring of cecal content as
133 fat or water. In GF mice, fat mass readout by EchoMRI decreased from 0.2 g to 2.3 g (Suppl. Fig.
134 1F) when comparing values with and without the cecum. This represented between 5 to 48% of

135 the original fat mass readout. We also observed a shift towards *higher* fat mass readings in SPF
136 mice after cecum removal (Suppl. Fig. 1F and Suppl. Fig. 1G); further highlighting the need for
137 caution in interpreting EchoMRI readouts for fat mass in mice with major differences in intestinal
138 colonization. Therefore, we proceeded to directly weigh the fat depots accessible to dissection
139 (interscapular brown adipose tissue, iBAT; and, inguinal and visceral white adipose tissue, iWAT
140 and vWAT) as a more reliable method. There was no significant difference between GF and SPF
141 mice in size of the explored fat depots; however, OligoMM12 mice accumulated more fat in all
142 explored depots than GF mice, and more iBAT and vWAT compared to SPF mice (Fig 1G).

143 **Energy metabolism and energy balance in GF, OligoMM12 and SPF mice**

144 In order to explain the body composition differences observed in the GF, OligoMM12 and SPF
145 mice, we explored the daily energy expenditure of these mice. Energy expenditure was estimated
146 using VO_2 and VCO_2 readouts (Meyer et al., 2015) and normalized as described before (Mina et
147 al., 2018; Speakman, 2013; Tschop et al., 2011) using lean body mass and dissected fat mass.
148 We could confirm that germ-free mice maintain their germ-free status over at least 10 days of
149 accommodation in these cages, via culture-dependent and culture-independent techniques (see
150 Methods).

151 In contrast to some previous reports (Bäckhed et al., 2004; Levenson, 1978; Li et al., 2019;
152 Wostmann et al., 1968), but aligned with others (Krisko et al., 2020; Kübeck et al., 2016), we found
153 no significant difference in daily energy expenditure (Fig. 2A and Fig. 2B) or VO_2 (Suppl. Fig. 2A
154 and Suppl. Fig. 2B) between GF, OligoMM12 and SPF mice after normalization using a regression
155 model that included lean body mass and total dissected fat mass as predictive variables. This lack
156 of difference was also observed when light and dark phases were analyzed separately (Fig. 2B
157 and Suppl. Fig. 2B). “Classical” normalization procedures (dividing by mass) also showed no
158 difference between groups when lean body mass, or “total body mass after cecum dissection” was

159 used for normalization of energy expenditure (Fig. 2C and D) or VO_2 (Suppl. Fig. 2C and D).
160 Unsurprisingly, we did find a significant difference during the dark phase in energy expenditure
161 (Fig. 2E) and VO_2 (Suppl. Fig. 2E) between GF and SPF mice if "total body mass" (i.e., including
162 cecum mass) was used for normalization, as on average 10% of total body mass in GF mice
163 comprises the non-metabolically active sterile cecal mass (compared to the 2.5% in SPF mice,
164 Suppl. Fig.1A). Therefore, at least when comparing to the SPF microbiota used in this study,
165 absence of a microbiota does not result in altered daily energy expenditure in metabolically active
166 tissues.

167 We hypothesized that adiposity in the OligoMM12 mice can be due to increased calorie absorption
168 from food. This was assessed by comparing the daily energy ingestion from food and calorie
169 excretion in feces, in GF, OligoMM12 and SPF mice. The difference between these two values
170 estimates the absorbed calories. As reported previously (Wostmann et al., 1983), GF animals
171 ingested on average between 10-20% more standard chow compared to OligoMM12 and SPF
172 mice (Fig. 2F). Correspondingly, GF animals also excreted a much larger dry mass of feces, while
173 OligoMM12 mice produced an intermediate fecal mass and SPF mice excreted the least (Fig. 2G).

174 Remarkably, energy density of dry feces was lower in GF mice (3.7 Kcal/g) compared to colonized
175 mice (OligoMM12 and SPF, 4.0 Kcal/g); with the latter showing no difference among them (Fig.
176 2H). This gap between GF and mice with microbiota can likely be explained by the fact that
177 although fecal bacteria improve energy release from food, a considerable fraction of that energy
178 remains stored in the bacteria present in the feces. Assuming certain averaged parameters (dry
179 mass of a bacterium = 2.26×10^{-13}g / bacteria cell (Dennis and Bremer, 2008), density of bacteria
180 in feces = 5×10^{11} bacteria cells / g of feces (Barlow et al., 2020), and energy stored in bacteria =
181 4.58 Kcal/g of dry bacteria mass (Popovic, 2019)); we estimated that the fecal microbiota of
182 colonized mice can contribute approx. 0.52 Kcal/g of dry fecal mass – slightly more than the energy
183 density difference between fecal energy density in colonized and germ-free mice.

184 We then used these values for food intake, fecal dry mass output, and fecal energy density to
185 estimate energy absorbed from the feces. We found that the higher food consumption in GF mice
186 (Fig. 2I) almost perfectly counterbalance their corresponding higher energy excretion in feces (Fig.
187 2J), such that all mice extract around 9 Kcal per day from their food (Fig. 2K). This is consistent
188 with our measurements of daily energy expenditure by indirect calorimetry (Fig. 2B), although it
189 fails to explain the observed adiposity in the OligoMM12 mice (Fig. 1G). Unexpectedly, the
190 OligoMM12 microbiota does not fully recapitulate the ability of a complex microbiota to improve
191 energy availability from food, as the fraction of all calories extracted from consumed food remains
192 similar between germ-free and OligoMM12 mice. Given that the gut content of both OligoMM12
193 and SPF mice is densely colonized, and the fecal energy density is similar; it should be noted that
194 the lower amount of energy extracted by the OligoMM12 is not so much due to a poorer digestive
195 capacity of the gnotobiotic gut microbes, but rather that compared to the SPF microbiota, the
196 calories extracted by the OligoMM12 microbiota are either retained within the microbes or not
197 converted into compounds that can be taken up by their host (Fig. 2L).

198 We therefore concluded that daily energy expenditure and daily energy absorption from food
199 varies only within the range of experimental error intrinsic to indirect calorimetry experiments. At
200 a fundamental level, food intake therefore seems to be well regulated by microbiota-released
201 calories. Despite this, OligoMM12 mice have an elevated fat mass. It remains a distinct possibility
202 that gain of fat mass depends on the cumulative effect of minute differences in energy intake and
203 energy expenditure that are simply not resolvable in our system. Nevertheless, in order to gain a
204 deeper insight into underlying mechanisms we carried out a series of more detailed analyses of
205 metabolism.

206 **Circadian changes in RER and microbiota-derived hydrogen and short-chain fatty acids**
207 **(SCFA)**

208 The tight control of eating behavior based on absorbed calories with or without a microbiota is
209 even more impressive when one considers the difference in substrates being used for oxidative
210 metabolism and the timing of their arrival in the circulation with relation to eating. Respiratory
211 exchange ratio (RER, the ratio of CO_2 produced per O_2 consumed) is widely used as an
212 informative proxy for substrate utilization (i.e., glucose or fatty acids) for oxidation in tissues. In
213 general, GF mice have a lower RER compared to SPF in both light and dark phases, potentially
214 explained by increased fat/decreased glucose metabolism in GF mice (Fig 3A). Therefore,
215 appetite regulation functions despite very different metabolic substrate availability in GF and SPF
216 mice. Intriguingly, OligoMM12 mice displayed an RER at the GF level during the light phase (when
217 mice typically sleep and fast) but raised up to SPF levels during the dark phase (i.e., when mice
218 are active and eating). It therefore appears that the OligoMM12 microbiota better recapitulates the
219 microbiome effects on the host during the dark (active) phase when food-derived carbohydrates
220 are abundant in the large intestine, but not when mainly host-derived carbon sources are available
221 in the large intestine (Fig. 3A). These changes in RER are not related to differences in feeding
222 patterns as all mice have a similar food intake during the periods in which their RERs differ the
223 most (Fig. 3B).

224 Differences in RER provided a clue that there could be differences in energy storage in mice with
225 different microbiota status. Microbial fermentation products, including short-chain fatty acids
226 (SCFA) and lactate, can be directly used as energy and carbon-sources by the murine host, and
227 are generated by the microbiota via processes that liberate molecular hydrogen. We therefore
228 quantified hepatic concentrations of glycogen, and cecal concentrations SCFA, at Zeitgeber 5
229 (ZT5, 5h into the light phase) and 16 (ZT16, 4h into the dark phase). Hydrogen was measured
230 continuously during the circadian cycle.

231 Hepatic glycogen levels show a circadian rhythm, which usually peaks early during the transition
232 between dark to light phase (ZT2-4), and drops to its minimum during the early hours of the dark

233 phase (ZT14-16) in nocturnal rodents (Doi et al., 2010; Ishikawa and Shimazu, 1976). We found
234 similar accumulation of hepatic glycogen in GF, OligoMM12 and SPF mice at ZT5; however, GF
235 and OligoMM12 mice drop to lower levels of hepatic glycogen compared to SPF mice at ZT16 (Fig
236 3C). This differential pattern in GF/OligoMM12 compared to SPF mice may indicate that, although
237 they can equally fill up hepatic glycogen storages at the end of the dark phase, GF and OligoMM12
238 show faster depletion of hepatic glycogen during the light phase.

239 Hydrogen, a byproduct of fiber fermentation by the microbiota, was also measured in the exhaust
240 air of the metabolic cages. We found a clear circadian pattern in hydrogen production between
241 OligoMM12 and SPF mice (Fig. 3D). Hydrogen levels in OligoMM12 and SPF mice decreased
242 down to the limit of blank (GF level as reference) during the light phase, to later peak after food
243 intake resumes during the dark phase. In addition, OligoMM12 mice showed a higher production
244 of hydrogen than SPF mice during the dark phase even after regression-based normalization by
245 cecal mass, which is larger in OligoMM12 mice (Fig. 3D). Therefore, the higher dark phase
246 hydrogen measurements in the OligoMM12 mice are not just the result of a larger cecal mass, but
247 of the OligoMM12 microbiota producing hydrogen at a higher rate per cecal content mass than
248 the SPF microbiota.

249 SCFA are the other major output of bacterial fermentation in the large intestine, as well as being
250 key bioactive compounds produced by the large intestinal microbiota. SPF mice showed the
251 highest cecal concentrations of all SCFA during both the light phase (butyrate and propionate)
252 and dark phase (acetate, butyrate, and propionate). Interestingly, OligoMM12 mice showed only
253 20-50% of the SCFA concentrations observed in SPF mice but instead showed high production of
254 lactate during the dark phase (Fig. 3E). In germ-free mice, all analyzed metabolites had levels
255 below the limit of blank except for lactate, which could correspond to host-produced L-lactate
256 (Zarrinpar et al., 2018) (our assay is not able to differentiate the enantiomers). As the total mass
257 of cecum content is widely different among GF, OligoMM12 and SPF mice, we also estimated the

258 total quantity of each compound in the cecal content by multiplying the concentration (Fig. 3E) by
259 the cecal mass for each group (Fig. 1C) while propagating the uncertainty of each measurement,
260 as a way of representing the total availability of SCFA for the different hosts. This transformation
261 has quite a major impact on how these data can be interpreted: when taking cecal mass into
262 account, OligoMM12 mice have considerably higher levels of acetate during the light and dark
263 phase and of propionate during the light phase than SPF mice, while butyrate levels remain low.
264 There is also an increased abundance of lactate and succinate in the OligoMM12 cecum content
265 (Fig. 3F). Although we cannot directly link these microbial metabolites to the phenotype of the
266 OligoMM12 mice, this underlines the major differences in metabolite profiles in the large intestine
267 when comparing germ-free, gnotobiotic and SPF mice. High lactate production by the microbiome
268 certainly warrants further study for potential metabolic effects on the host.

269 **Circadian changes in liver and plasma metabolites in GF, OligoMM12 and SPF mice**

270 Finally, to increase our metabolic resolution, we applied UPLC-MS to perform untargeted
271 metabolomics in the liver and plasma during the light (Zeitgeber 5) and dark phase (Zeitgeber 16)
272 in GF, OligoMM12 and SPF mice. Hierarchical clustering (Fig. 4A and Fig. 4C) and PCA analysis
273 (Fig. 4B and Fig. 4D) separate the SPF, OligoMM12 and GF groups during both light and dark
274 phases. Correlating to what we observed in the RER during the light phase, GF and OligoMM12
275 cluster closer and are clearly separated from the SPF in the light phase PCA analysis for both liver
276 (Fig. 4B) and plasma samples (Fig. 4D). During the dark phase, although OligoMM12 mice
277 differentiate from GF, they do not recapitulate the metabolome of SPF mice neither in liver (Fig.
278 4B) or plasma samples (Fig. 4D).

279 We used the package MetaboAnalystR (Chong and Xia, 2018) to identify compounds that are
280 significantly different in pair comparisons between OligoMM12 mice and their GF and SPF
281 counterparts by untargeted peak extraction and map them into metabolic pathways using the

282 KEGG database. We found several pathways differentially enriched when OligoMM12 mice were
283 compared to GF or SPF counterparts during the light and dark phase in liver (Fig. 4E) and plasma
284 (Fig. 4F), including amino acid, bile acids, and fatty acid metabolism. Additionally, we selected
285 compounds that belong to these differentially enriched pathways or have been previously
286 identified to have circadian changes in obese patients (Nowak, 2021), confirmed their structure by
287 using chemical standards, and performed a targeted peak extraction for a more precise
288 comparison among groups (Suppl. Table 1). For certain metabolites the OligoMM12 microbiota
289 produce an intermediate phenotype between GF and SPF mice, e.g., a subset of bile acids, in
290 liver (Suppl. Fig 3A) and plasma (Suppl. Fig 3B).

291 **DISCUSSION**

292 Since the early days of nutritional studies, there has been a clear interest to understand the role
293 of microbiota in host morphology, physiology and nutrition (Gordon and Pesti, 1971; Levenson,
294 1978). Pioneering work comparing germ-free animals with conventionally raised or gnotobiotic
295 counterparts already described differences in food intake, energy extraction from diet and energy
296 expenditure by indirect calorimetry (Levenson et al., 1969; Wostmann et al., 1983). More recently,
297 researchers have explored the effect of specific microbiota communities and how they influence
298 energy metabolism and body composition in the host (Ridaura et al., 2013; Suárez-Zamorano et
299 al., 2015; Turnbaugh et al., 2006).

300 Here, by carefully checking the validity of different measurement types, we found no significant
301 difference in lean body mass among germ-free (GF), gnotobiotic (OligoMM12) and conventionally
302 raised (SPF) mice. Interestingly, there was a significant increase in fat depots in OligoMM12 mice
303 compared to GF and SPF animals. Previous studies diverged on the effect of microbiota on fat
304 mass accumulation during conventional/low-fat diet feeding; reporting either increased fat mass
305 in SPF mice (Bäckhed et al., 2004) or no difference compared to GF mice (Kübeck et al., 2016).
306 However, it should be noted that there can be huge differences between SPF microbiota within
307 and between animal facilities. GF mice transplanted with microbiota derived from obese donors
308 accumulated more fat mass compared to those transplanted with microbiota derived from lean
309 donors (Halatchev et al., 2019; Ridaura et al., 2013; Turnbaugh et al., 2006), with correlates
310 identified to individual species/strain abundance (Woting et al., 2014, 2015). SPF microbiota
311 matching more closely to those from obese donors could therefore be expected to give differing
312 results to ours. In contrast, minimal microbiota communities can be perfectly replicated across
313 sites, and can help to clarify the complex processes linking microbiota and host metabolism
314 (Becker et al., 2011). Further exploration of the metabolic effects of the OligoMM12 microbiota
315 community, and extended versions thereof, has potential to clarify if specific strains, species or

316 functional classes (Schmidt et al., 2018) are sufficient and necessary to drive the development of
317 increased fat depots in these mice.

318 Our analysis compared energy expenditure in GF, OligoMM12 and SPF mice and found no
319 significant difference among these mice. Normalization of mass-dependent variables by a per-
320 mass (or allometric transformation) ratio has been recognized as a common source of controversy
321 (Packard and Boardman, 1999; Tanner, 1949; White and Seymour, 2005), especially with large
322 changes in body mass composition (Butler and Kozak, 2010; Kaiyala and Schwartz, 2011), and
323 there have been several publications calling for the use of better statistical methods (Arch et al.,
324 2006; Fernández-Verdejo et al., 2019; Tschop et al., 2011). We found that, when the cecal content
325 mass is very different among groups, using total body mass for normalization introduces a
326 considerable bias in normalized energy expenditure estimation. Interestingly, it was long-ago
327 observed that surgical removal of the cecum equalized the oxygen consumption between germ-
328 free and conventional rats; as well as other measurements normalized by total body mass
329 (Wostmann et al., 1968). With normalization using linear regression models based on lean-mass
330 and fat-mass (Mina et al., 2018), we and others found no significant differences in energy
331 expenditure by indirect calorimetry between GF and SPF mice under standard chow diet
332 conditions (Krisko et al., 2020; Kübeck et al., 2016; Li et al., 2021). Importantly, we suggest
333 cautious interpretation of lean and fat mass readouts obtained by EchoMRI when comparing mice
334 with major differences in intestinal content composition. We are also keen to point out the more
335 general limitations of our observations: only one gnotobiotic microbiota and one SPF microbiota
336 were analyzed, and our conclusions pertain exclusively to these. We in no way exclude the
337 possibility that some microbiota constituents or conformations *can* influence host energy
338 expenditure (Halatchev et al., 2019) and/or body composition (Ridaura et al., 2013; von
339 Schwartzenberg et al., 2021; Turnbaugh et al., 2006). In addition, it should be noted that indirect

340 calorimetry is an inherently noisy data type, and small differences in daily energy expenditure are
341 impossible to resolve via this technique (Corrigan et al., 2020; Fernández-Verdejo et al., 2019).

342 Nevertheless, the lack of measurable difference in energy expenditure between GF, OligoMM12
343 and SPF mice is aligned with our finding that the amount of energy obtained by *ad libitum* food
344 intake was also remarkably similar among the groups. GF mice seem to accurately compensate
345 the lower capacity of energy extraction from diet by increasing food intake. While this seems
346 generally to be in agreement with models that described the regulation of appetite (and therefore
347 energy intake) by the basal energy requirement of the individual (MacLean et al., 2017; Stubbs et
348 al., 2018), it remains surprising given the discrepancy in the types of substrates available for
349 oxidative metabolism in colonized and germ-free mice. Although germ-free mice have a longer
350 total gastrointestinal transit time than SPF mice (Touw et al., 2017), very little calorie absorption
351 from food can occur after ingested food reaches the cecum of a germ-free mouse, whilst an SPF
352 mouse will release usable energy from their food via microbial fermentation for several more hours
353 in the cecum and colon, generating a major time-difference in the absorption of calories after
354 eating in germ-free and SPF animals. This compensation seems also to function in mice colonized
355 with the OligoMM12 microbiota, where despite robust microbial fermentation (read out as
356 hydrogen and fermentation product production) and identical fecal energy density to SPF mice,
357 energy recovery from ingested food is poor due to the volume of feces shed. A clear conclusion
358 from these observations is that microbiota-dependent changes in metabolic substrates, and timing
359 of calorie absorption, are well integrated in the murine central regulation of appetite over the
360 course of a day (Fetissov, 2017).

361 Despite this broadly successful regulation of food intake and energy expenditure, at the molecular
362 level, major differences were observed between the mice with different microbiota. In cecum
363 content, the OligoMM12 microbiota was associated with a predominance of succinate and lactate,
364 at the expense of propionate and butyrate. In complex microbiotas, lactate is typically further

365 metabolized to butyrate by specific firmicutes (Belenguer et al., 2011; Duncan et al., 2004; Flint et
366 al., 2015), which may be lacking or insufficiently abundant in the OligoMM12 mice. As lactate can
367 inhibit lipolysis in adipocytes (Cai et al., 2008; Liu et al., 2009), this raises an interesting theme for
368 follow-up studies to define the role of microbiota-derived lactate in host metabolism. In line with
369 the RER data, we also observed that the liver and plasma metabolite profiles of OligoMM12 mice
370 clustered closer to GF mice than to SPF mice. Although certain compounds were differentially
371 represented between OligoMM12 and GF or SPF mice, we could not replicate earlier observations
372 (Claus et al., 2008; Mardinoglu et al., 2015). This discrepancy may be explained by the location
373 of the sample collection (portal vein vs. liver/peripheral plasma) or the lack of power of our sample
374 size to detect significant differences having both circadian phase and microbiota as covariables.
375 Interestingly, OligoMM12 had a bile acid profile closer to GF than SPF mice, for example showing
376 GF-levels of β-murocholic acid, the predominant bile acid in the liver of GF mice (Sayin et al.,
377 2013). Follow up studies with manipulation of the OligoMM12 microbiota or metabolic interventions
378 are a promising tool to pull apart the circadian effects on RER, the influence of an unusual
379 fermentation product profile, and other more subtle metabolic changes on overall metabolic health
380 of the murine host.

381 In conclusion, our study showed that isolator-based indirect calorimetry is possible and allows
382 detailed analysis of the metabolism of germ-free and gnotobiotic mice in real-time. Data generated
383 with this system demonstrated that microbiota-released calories are well integrated in host energy
384 balance. Intriguingly, the OligoMM12 gnotobiotic microbiota accumulate fat mass, and displays a
385 GF-like RER during the light phase but an SPF-like RER during the dark phase. The OligoMM12
386 mice have a skewed profile of cecal fermentation products during both light and dark phases,
387 including very high concentrations of lactate, as well as alterations in bile acid, fatty acid and amino
388 acid metabolism in blood and liver. This reveals the full potential for gnotobiotic microbiota
389 communities to investigate the mechanisms underlying the influence of microbiota composition

390 and function on host metabolic health. As microbial dysbiosis is associated with a range of human
391 diseases, circadian analysis of energy balance represents a crucial tool in the mining of
392 microbiome data for therapeutic and diagnostic purposes.

ACKNOWLEDGEMENTS

We would like to thanks to Sven Nowok, Thomas Fehr, Andre Galhano and Susanne Freedrich for their support in the establishment of the gnotobiotic metabolic phenotype facility in the ETH Phenomic Center. Also, we thank Maria L. Balmer for her comments and suggestions for the manuscript. The gnotobiotic metabolic phenotype facility was initially funded by the FreeNovation grant (Novartis). E.S. and W-D.H. are supported by the NCCR Microbiomes, a research consortium financed by the SNF. E.S. acknowledges the support of the Swiss National Science Foundation (40B2-0_180953, 310030_185128), European Research Council Consolidator Grant, and Gebert Rüf Microbials (GR073_17) and the Botnar Research Centre for Child Health Multi-Invesitigator Project 2020. This project is part of "Zurich Exhalomics", a flagship project of “Hochschulmedizin Zürich”.

Author Contributions

Conceptualization, D.H., W-D.H., C.W. and E.S.; Methodology, D.H., J.L., W.S., R.Z. C.W. and E.S.; Formal Analysis, D.H., J.L, W.S., T.G. and M.A.; Investigation, D.H., J.L., W.S. and S.N.; Resources, B.S., R.Z., W-D.H., C.W. and E.S.; Writing – Original draft, D.H. and E.S.; Writing – Review and Editing D.H., J.L., W.S, T.G, M.A, S.N., A.J.M., B.S., R.Z., W-D.H., C.W and E.S.; Visualization, D.H., W-D.H., C.W. and E.S.; Supervision, W-D.H., C.W. and E.S.; Funding acquisition, W-D.H., C.W., A.J.M, and E.S.

Declaration of Interest

The authors declare no competing interests.

413 **FIGURES TITLES AND LEGENDS**

414 **Figure 1: OligoMM12 mice have increase fat mass compared to GF mice and SPF C57B6/J**
415 **mice.** (A) Schematic representation of isolator-based indirect calorimetry system, with a TSE
416 PhenoMaster® calorimeter connected to two flexible surgical isolators with four metabolic cages
417 each. (B) Pictures of isolator-based indirect calorimetry system inside the facility. (C) Cecal mass
418 (tissue including luminal content). (D) Total body mass at the end of the experiment and before
419 cecum removal. (E) Total body mass after cecum removal. (F) Lean body mass acquired by
420 EchoMRI before cecum removal (N of mice per group with EchoMRI and indirect calorimetry
421 measurements: GF = 12, OligoMM12 = 8, SPF = 11). (G) Fat mass from interscapular brown
422 adipose tissue (iBAT), inguinal white adipose tissue (iWAT) and visceral white adipose tissue
423 (vWAT). Number of mice per group in all figures unless otherwise specified: GF = 16, OligoMM12
424 = 12, SPF = 11. p-values obtained by Tukey's honest significance test.

425 **Figure 2: Energy metabolism in GF, OligoMM12 and SPF C57B6/J mice.** (A) Linear regression
426 of energy expenditure and lean body mass based on EchoMRI during light and dark phase. Each
427 colored vertical line represents energy expenditure measurements during the experiment for one
428 mouse. (B) Energy expenditure during 24h period, or during the 12h light or dark phase. Values
429 represent area-under-curve normalized by regression-based analysis using lean body mass
430 obtained by EchoMRI and dissected fat mass. (C, D, E) Energy expenditure values obtained by
431 “classical” ratio-based normalization methods (dividing energy expenditure values per phase by
432 mass). (C) Area-under-curve after normalization by total mass after cecal dissection. (D) Area-
433 under-curve after normalization by lean body mass (EchoMRI). (E) Area-under-curve after
434 normalization by total body mass before cecal dissection. (F) Average daily food intake per mouse.
435 Mice represented in this figure include those that underwent long-term indirect calorimetry (Fig. 3)
436 and mice that only contribute to daily fecal pellet quantification/bomb calorimetry. (N of mice per
437 group: GF = 24, OligoMM12 = 19, SPF = 10) (G) Dry fecal output per mouse collected during a

438 24h period. (N of mice per group: GF = 12, OligoMM12 = 8, SPF = 4) (H) Energy content of dry
439 fecal output by bomb calorimetry. (N of mice per group: GF = 21, OligoMM12 = 11, SPF = 11). (I,
440 J, K, L) Estimation energy metabolism parameters. Number represented estimate mean value ±
441 1.96*combined standard uncertainty from measurements used for calculations. (I) Estimated daily
442 energy input (food intake* 3.94 Kcal/g). (J) Estimated daily energy excretion (daily fecal dry
443 mass*fecal energy content). (K) Estimated daily energy extraction (daily energy input – daily
444 energy excretion). (L) Estimated energy extraction from food as percentage of energy input ((daily
445 energy input - daily energy excretion)/daily energy input*100). Note that calculations in L, N and
446 M are per mouse and are not normalized to body mass. Number of mice per group in all figures
447 unless otherwise specified: GF = 9, OligoMM12 = 8, SPF = 10. p-values obtained by Tukey's
448 honest significance test.

449 **Figure 3: Circadian changes in Respiratory Exchange Ratio (RER), microbiota-derived**
450 **hydrogen and short-chain fatty acids (SCFAs).** (A) Comparison of circadian changes in RER
451 among GF, OligoMM12 and SPF C57B6/J mice. RER curves obtained by smoothing function of
452 data obtained every 24min per mouse over 10 days. Mean RER during the light phase (Zeitgeber
453 0-12) and dark phase (Zeitgeber 12-24). (B) Cumulative food intake during described ZT periods.
454 Mice included in this analysis are those that underwent long-term indirect calorimetry, and they
455 are a subset of the mice represented in Fig. 2F (C) Hepatic glycogen and triglyceride concentration
456 in samples obtained at Zeitgeber 5 and 16 (N=3 per group). (D) Hydrogen production, curves
457 obtained by smoothing function of data obtained every 24min per mouse. Area-under-curve after
458 regression-based normalization by cecal mass during the light and dark phase (N of mice per
459 group: OligoMM12 = 11, SPF = 10). (E) Concentration of short-chain fatty acids (acetate, butyrate,
460 propionate) and intermediate metabolites (lactate, succinate) products in cecal content (N=3 per
461 group). (F) Estimation total amount of short-chain fatty acids and intermediate metabolites by
462 multiplying measured concentration values by the cecal mass of the group. Number represented

463 estimate mean value ± combined standard uncertainty from measurements used for calculations.
464 Number of mice per group in all figures unless otherwise specified: GF = 13, OligoMM12 = 12,
465 SPF = 10. p-values obtained by Tukey's honest significance test.

466 **Figure 4. Metabolic profile comparison of GF, OligoMM12 and SPF C57B6/J mice by**
467 **UPLC/MS**. (A and C) Heatmaps of metabolites identified by untargeted UPLC/MS during the light
468 phase (Zeitgeber 5) and dark phase (Zeitgeber 16) in (A) liver and (C) plasma. (B and D) PCA
469 analysis of metabolites identified by untargeted UPLC/MS during the light phase (Zeitgeber 5) and
470 dark phase (Zeitgeber 16) in (B) liver and (D) plasma. (E and F) Metabolic pathways identified in
471 the KEGG PATHWAY database; red dots represent pathways containing compounds differentially
472 enriched in (*top*) OligoMM12 vs. GF and (*bottom*) OligoMM12 vs. SPF comparisons. Samples
473 obtained during the light phase (Zeitgeber 5) and dark phase (Zeitgeber 16) in (E) liver and (F)
474 plasma. Number of mice per group in all figures: GF = 3, OligoMM12 = 3, SPF = 3.

475 **METHODS**

476 **Animals**

477 We used C57B6/J male mice aged between 12-14 weeks. We compare germ-free mice (GF), with
478 a 12-strain gnotobiotic microbiota (Brugiroux et al., 2016) (OligoMM12) and specific-pathogen free
479 mice (SPF). GF and OligoMM12 mouse lines are bred and maintained in open-top cages within
480 flexible-film isolators, supplied with HEPA-filtered air, and autoclaved food and water ad libitum.
481 As we are aware that housing conditions may influence behavior and potentially metabolism, we
482 also bred and maintained a SPF colony under identical conditions inside a flexible-film isolator
483 specifically for this study, such that all mice experienced identical living conditions, food, and water.
484 Mice were adapted for between 24-36h after transfer from the breeding isolators to the isolator-
485 based metabolic chambers. For long term experiments, mice were periodically re-housed in
486 couples for short periods of times to avoid stress of extended single-housing conditions. In all
487 cases, animals were maintained with standard chow (diet 3807, Kliba-Nafag, Switzerland) and
488 autoclaved water. Germ-free status was confirmed at the end of the long-term experiments by
489 culturing cecal content in sterile BHIS media in aerobic and anaerobic conditions for a week. In
490 addition, cecal content was frozen at -20°C for a week, then stained with SYBR Gold and assessed
491 by bacterial flow cytometry (Moor et al., 2016) using similarly processed SPF mice cecal content
492 as positive control for the presence of bacteria. All experiments were conducted in accordance
493 with the ethical permission of the Zürich Cantonal Authority.

494 **Indirect calorimetry**

495 The isolator-housed TSE PhenoMaster® system allows instantaneous measurements of oxygen,
496 carbon dioxide and hydrogen levels as well as total feed and water consumption while keeping a
497 strict hygiene level of control. The metabolic isolator system consists of an adapted set of two

498 flexible-film surgical isolators, each of them housing four metabolic cages from the TSE
499 PhenoMaster® system (TSE Systems, Germany). Room air is pulled into the isolator by a vacuum
500 pump passing through a double set of HEPA filters. Then, each cage is connected via a second
501 HEPA filter through the back wall of the isolator to the CaloSys setup, which pulls sterile air from
502 the isolator into the cages using negative pressure. Air coming from the cages is dehumidified at
503 4°C and sequentially passed by a Sensepoint XCD Hydrogen gas analyzer (Honeywell Analytics,
504 Hegnau, Switzerland) and standard oxygen and carbon dioxide censors provided in the TSE
505 PhenoMaster® system. A two-point calibration of all analyzers using reference gases was
506 performed within 24 h before each animal experiment. Data was recorded using a customized
507 version of the TSE PhenoMaster® software modified to integrate hydrogen measurements.

508 For indirect calorimetry measurements, the animals were transported in pre-autoclaved, sealed
509 transport cages from the breeding isolators into the metabolic isolator system. Mice were single
510 housed and adapted for between 24-36h before starting recording measurements to ensure
511 proper access to food and water as well as account for initial exploratory behavior. Mice were kept
512 up to 10 days at a stable temperature (21-22°C) with *ad libitum* availability of standard chow and
513 water. The days were divided into a dark and light period of 12 hours each. In this study, we kept
514 the air flow of 0.4 L/min and recorded individual cage data (gases production and food/water
515 consumption) every 24min (time set per cage for measurement stabilization 2.5min). In long
516 experiments, mice were periodically pair-housed for 24h to prevent stress due to prolonged single
517 housing.

518 **Body composition measurements**

519 At the end of the experiment, mice were fasted for 4 hours (Zeitgeber 1 till 5) before for body
520 composition measurements. We used magnetic-resonance whole-body composition analyzer
521 (EchoMRI, Houston, USA) to analyze mice body composition (lean and fat mass). Then, mice

522 were euthanized using CO_2 according to approved protocols. Total body mass was obtained by
523 weighing the full carcass and cecum was dissected and weighed by one investigator (DH). For a
524 set of mice, we remeasured body composition by EchoMRI after cecum removal. Finally, fat
525 depots were dissected from all mice by one investigator (W.S.) that was blinded to the hygiene
526 status of the mice. Interscapular brown adipose tissue (iBAT), inguinal white adipose tissue (iWAT)
527 and visceral white adipose tissue (vWAT) were sampled and weighted.

528 **Food intake, fecal samples and bomb calorimetry**

529 Daily food intake was obtained as the mean value of food intake recorded by the TSE
530 PhenoMaster® system during the course of the experiment. In addition to the mice reported in the
531 indirect calorimetry experiments, we also collected food intake data from a set of selected
532 experiments in which we collected fecal pellets produced during 24h. For daily fecal excretion
533 measurements, we cleaned up the bedding in the cage and replaced it for a clean and reduced
534 amount of bedding. After 24h, we collected the mix of bedding and fecal pellets. Fecal pellets were
535 manually collected from the bedding, transferred to 15ml tubes and stored at -20°C until bomb
536 calorimetry. Before bomb calorimetry, fecal samples were freeze dried in a lyophilizer overnight
537 (ALPHA 2-4 LDplus, Christ, Germany) and dry mass recorded. We used a C1 static jacket oxygen
538 bomb calorimeter (IKA, Germany) to quantify the residual energy present in these dry fecal pellets,
539 using approximately 0.2-0.5g of material. Energy content was normalized to grams of dry fecal
540 pellets.

541 **Metabolomics by UPLC/MS**

542 *Sample obtention and preparation*

543 Approximately at Zeitgeber 5 and 16, three mice of each group were euthanized, and liver and
544 plasma samples collected. To minimize variations among mice, individual mice were euthanized
545 with CO_2 and sampled as fast as possible. Blood was obtained by cardiac puncture, collected in
546 lithium heparin coated tubes, and kept on ice for further processing. Mice were perfused with PBS
547 and liver samples were obtained by dissection of the lower right lobe, collected on an 2ml
548 Eppendorf tube and flash frozen in liquid nitrogen. Finally, between 60-80 mg of cecal content was
549 collected in a 2ml Eppendorf tube and flash frozen in liquid nitrogen. After samples all samples
550 were obtained, blood samples were centrifuged 8000rcf for 5min, supernatant collected, and flash
551 frozen in liquid nitrogen. Samples were kept at -80°C until preparation for UPLC/MS.

552 *Short chain fatty acid quantification by UPLC/MS*

553 Samples were first homogenized in 70%-isopropanol (1 mL per 10 mg sample), centrifuged.
554 Supernatants were used for SCFA quantification using a protocol similar to previously described
555 (Liebisch et al., 2019). Briefly, a 7-points calibration curve was prepared. Calibrators and samples
556 were spiked with mixture of isotope-labeled internal standards, derivatized to 3-
557 nitrophenylhydrazones, and the derivatization reaction was quenched by mixing with 0.1% formic
558 acid. Four µL of the reaction mixture was then injected into a UPLC-MS system, [M-H]- peaks of
559 the derivatized SCFAs were fragmented and characteristic MS2 peaks were used for
560 quantification.

561 *Untargeted UPLC/MS*

562 Samples were thawed on ice. Serum samples were diluted with 90% methanol in water with a
563 volumetric ratio of 1:7, incubated for 10 min on ice for allowing protein to precipitate. Liver samples
564 were mixed with 75% methanol in water (2 mL/ 100 mg liver), homogenized using a TissueLyser
565 (Qiagen, Germany) at 25 Hz for 5 min. The result mixtures were centrifuged at 15,800 g, 4 °C for

566 15 min. 100 µL of the supernatants were filtered with 0.2 µm reversed cellulose membrane filter
567 and transferred to sample vials and used for UPLC/MS analysis with an ACQUITY UPLC BEH
568 AMIDE column (1.7 µm, 2.1 × 150 mm, Waters). Another 400 µL of the supernatants were then
569 lyophilized and resuspended in 80 µL 5% methanol in water, sonicated, filtered, and used for
570 UPLC/MS analysis with an ACQUITY UPLC BEH C18 column (1.7 µm, 2.1 × 150 mm, Waters,
571 RP column).

572 An ACQUITY UPLC system (I-Class, Waters, MA, USA) coupled with an Orbitrap Q-Exactive Plus
573 mass spectrometer (Thermo Scientific, San Jose, CA) were used for UPLC/MS analysis. For the
574 AMIDE column a flow rate of 400 µL/min was used with a binary mixture of solvent A (water with
575 0.1% formic acid) and solvent B (acetonitrile with 0.1% formic acid). The gradient starts from 1%
576 of A, then gradually increases to 70% of A within 7 min. Then a 1% of A is kept for 3 min. The
577 column was kept at 45 °C and the autosampler at 5° C.

578 For the RP column, the flow rate was set to 240 µL/min using a binary mixture of solvent A (water
579 with 5 % methanol and 0.1 % formic acid) and solvent B (methanol with 0.1 % formic acid). The
580 gradient starts from 95% of A, then gradually decreases to 5% of A within 10 min. A 100% solvent
581 of B is kept for 2 min, then a 100% of A is kept for 2min to restore the gradient. The column was
582 kept at 30 °C and the autosampler at 5 °C.

583 The MS was operated at a resolution of 140,000 at m/z = 200, with automatic gain control target
584 of $2x10^5$ and maximum injection time was set to 100ms. The range of detection was set to m/z 50
585 to 750. Untargeted MS data was extracted from raw MS files by using XCMS (Smith et al., 2006)
586 in R (v3.6.1), and then subject to pathway enrichment by using MetaboAnalystR (Chong and Xia,
587 2018).

588 *Compound identification and targeted peak extraction*

589 Chemical standards of selected compounds were diluted to 10 µg/mL and were analyzed using
590 the UPLC/MS methods described before. Identification was done by comparing retention time and
591 MS2 in liver/plasma samples with the chemical standards (Nowak, 2021). After confirming the
592 chemical identities of the compounds, targeted peak extraction was done using Skyline (v21.1)
593 (Adams et al., 2020).

594 **Data Analysis**

595 *Data quality control*

596 To facilitate analysis across different experimental runs, all times were converted into Zeitgeber
597 time (ZT; [h]), where 0-12 represents the light phase and 12-24 represents the dark phase. Any
598 datapoint taken before the start of the first occurrence of ZT=0 was discarded. To account for
599 faulty measurements caused by measurement imprecision, equipment malfunction or other
600 disruptive events, datapoints were removed from the raw datasets according to criteria based on
601 statistical and biological arguments. Food consumption values of 0.01 g during the 24min intervals
602 were considered as measurement noise and discarded. Negative values for food and water
603 consumption, as well as oxygen (dO_2) and carbon dioxide (dCO_2) differentials between the
604 measurement chambers and the reference chamber were also considered as measurement noise
605 and discarded. For the remaining subsets of measurements from the individual mice, we cleaned
606 up outlier measurements in food and water intake by eliminating values greater than 75th percentile
607 + 1.5 times interquartile range. Potential sources for outlier measurements in food and water
608 consumption observed included leaky water bottles and loss of food pellets during mice husbandry
609 procedures. A similar approach was used to eliminate outliers from dO_2 and dCO_2 values below
610 25th percentile - 1.5 times interquartile range. Potential sources for outlier measurements in gas
611 differentials included inappropriate sealing of individual metabolic cages or clogging of pre-
612 analyzer filters. Oxygen consumption (VO_2) and CO_2 production (VCO_2) was calculated using dO_2

613 and dCO_2 and the Haldane transformation as described before (Arch et al., 2006). Energy
614 expenditure was estimated from dO_2 and dCO_2 using Weir's approximation (Weir, 1949). As one
615 of the study objectives is to explore circadian patterns, if more than 20% of datapoints had to be
616 removed from a particular day for a particular mouse, all other datapoints from that subset were
617 discarded as well. After the cleanup process described above, the data from all different
618 experiment runs were pooled together for further analysis. The above processes lead to a
619 reduction in dataset size from 10472 to 9453 entries.

620 *Statistical analysis*

621 From the resulting dataset, energy expenditure over a certain period was calculated as the area
622 under the curve (trapezoid interpolation) of instantaneous values obtained during the 24min
623 measurements intervals. Food intake values calculated over a certain time are always cumulative.
624 To compare different mice in the above variables, variations in body mass and composition
625 between individuals need to be accounted for. As suggested in several publications (Fernández-
626 Verdejo et al., 2019; Speakman, 2013; Tschop et al., 2011), this was done by regression-based
627 analysis of covariance (ANCOVA). As such, a linear regression is performed on energy
628 expenditure as a function of lean body mass and fat depots mass, with the microbiota group as a
629 qualitative covariate. Then, each individual value is replaced by the sum of the corresponding
630 residual and the energy expenditure predicted by the linear model using the average lean body
631 and fat depot mass (calculated over all groups). Hydrogen production (difference in hydrogen
632 concentration between the measurement chambers and the reference chamber) was adjusted in
633 analogous fashion, using cecal mass (as a proxy for total gut microbiota mass) as a predictor.

634 For variables where the continuous evolution during the circadian cycle is of interest (RER, gross
635 hydrogen production), values were averaged at each time point for each individual. A generalized

636 additive model was used to fit a smooth line to these averages using a cubic penalized regression
637 spline (using R function mgcv::gam with formula y ~ s(x; bs = “cs”)).

638 For estimating derived variables (i.e., daily energy excretion) we used the R package “errors”(Ucar
639 et al., 2019). This package links uncertainty metadata to quantity values (i.e., mean “daily fecal
640 dry mass excretion”, mean “fecal energy content”) and this uncertainty is automatically propagated
641 when calculating derived variables (i.e., “daily energy excretion” = “daily fecal dry mass excretion”
642 x “fecal energy content”). Uncertainty is treated as coming from Gaussian and linear sources and
643 propagates them using the first-order Taylor series method for propagation of uncertainty.

644 Hierarchical clustering and heatmap visualization were produced using the R package “pheatmap”
645 using Pearson correlation as distance measure for clustering and Ward's minimum variance
646 method using an algorithm that includes Ward’s criterion (Murtagh and Legendre, 2014). For the
647 Principal Component Analysis, we used the *prcomp* function which is present in built-in R stats
648 and the R package “factoextra” for visualization.

649 All group comparisons were analyzed by ANOVA and Tukey's honest significance test. For
650 comparisons of metabolites identified by targeted peak extraction among groups, area values
651 were log2 transformed before the statistical test.

652 **Resource availability**

653 *Lead contact*

654 Any further communication, including those related to resource sharing, may be directed to and
655 fulfilled by the lead contact Emma Slack (emma.slack@hest.ethz.ch).

656 *Materials availability*

This study did not generate new unique reagents.

Data and code availability

Source data for Fig. 1, 2 and 3, and Suppl. Fig. 1 and 2 are available in the Supplementary Information. Source data for Fig. 4 and Suppl. Fig. 3 and the datasets and code used for all figures in this publication are made available in a curated data archive at ETH Zurich (https://www.research-collection.ethz.ch/handle/20.500.11850/501168) under the DOI https://doi.org/10.3929/ethz-b-000501168.

664 **SUPPLEMENTAL INFORMATION TITLES AND LEGENDS**

665 **Supplementary Figure 1: Cecal mass interferes with fat mass estimation by EchoMRI.** (A)
666 Cecal mass (tissue including luminal content) as percentage of total body mass (N of mice per
667 group: GF = 16, OligoMM12 = 12, SPF = 11) (B) Lean body mass estimated by EchoMRI with and
668 without cecum. Equations show simple linear regression for estimating lean mass without cecum
669 based on lean mass with cecum; in brackets adjusted-R squared. (C) Lean mass variation after
670 cecum removal. (D) Lean mass variation after cecum removal as percentage of lean mass before
671 cecum removal. (E) Fat body mass estimated by EchoMRI with and without cecum. Equations
672 show simple linear regression for estimating fat mass without cecum based on fat mass with
673 cecum; in brackets adjusted-R squared. (F) Fat mass variation after cecum removal. (G) Fat mass
674 variation after cecum removal as percentage of lean mass before cecum removal. Number of mice
675 per group in all figures unless otherwise specified: GF = 13, OligoMM12 = 11, SPF = 15. p-values
676 obtained by Tukey's honest significance test.

677 **Supplementary Figure 2: Cecal mass interferes with normalization of VO_2.** (A) Linear
678 regression of VO_2 and lean body mass (EchoMRI) during light and dark phase. Each colored
679 vertical line represents energy expenditure measurements during the experiment per mouse. (B)
680 VO_2 during 24h period, or during the 12h light or dark phase. Values represent area-under-curve
681 normalized by regression-based analysis using lean body mass obtained by EchoMRI and
682 dissected fat mass (C, D, E) VO_2 values obtained by “classical” ratio-based normalization methods
683 (dividing energy expenditure values per phase by mass). (C) Area-under-curve after normalization
684 by total mass after cecal dissection. (D) Area-under-curve after normalization by lean body mass.
685 (E) Area-under-curve after normalization by total body mass before cecal dissection. Number of
686 mice per group in all figures unless otherwise specified: GF = 9, OligoMM12 = 8, SPF = 10. p-
687 values obtained by Tukey's honest significance test.

688 **Supplementary Figure 3. Metabolic profile comparison of GF, OligoMM12 and SPF C57B6/J**
689 **mice by UPLC/MS.** (A and B) Manually-curated list of compounds obtained by targeted peak
690 extraction from differentially expressed pathways in (A) liver and (B) plasma samples. p-values
691 obtained by Tukey's honest significance test after log2 transformation of area value.

692 **Supplementary Table 1. List of metabolites identified by targeted peak extraction in the**
693 **UPLC/MS data**. Table indicates compound name, KEGG Entry number, type of column was
694 used for UPLC and if the peak matched the retention time and MS2 spectra identified with the
695 chemical standard in liver and plasma samples.

REFERENCES

Adams, K.J., Pratt, B., Bose, N., Dubois, L.G., St John-Williams, L., Perrott, K.M., Ky, K., Kapahi, P., Sharma, V., MacCoss, M.J., et al. (2020). Skyline for Small Molecules: A Unifying Software Package for Quantitative Metabolomics. J. Proteome Res. *19*, 1447–1458, 10.1021/acs.jproteome.9b00640.

Arch, J.R.S., Hislop, D., Wang, S.J.Y., and Speakman, J.R. (2006). Some mathematical and technical issues in the measurement and interpretation of open-circuit indirect calorimetry in small animals. Int. J. Obes. (Lond). *30*, 1322–1331, 10.1038/sj.ijo.0803280.

Bäckhed, F., Ding, H., Wang, T., Hooper, L. V, Koh, G.Y., Nagy, A., Semenkovich, C.F., and Gordon, J.I. (2004). The gut microbiota as an environmental factor that regulates fat storage. Proc. Natl. Acad. Sci. U. S. A. *101*, 15718–15723, 10.1073/pnas.0407076101.

Bäckhed, F., Manchester, J.K., Semenkovich, C.F., and Gordon, J.I. (2007). Mechanisms underlying the resistance to diet-induced obesity in germ-free mice. Proc. Natl. Acad. Sci. U. S. A. *104*, 979–984, 10.1073/pnas.0605374104.

Barlow, J.T., Bogatyrev, S.R., and Ismagilov, R.F. (2020). A quantitative sequencing framework for absolute abundance measurements of mucosal and lumenal microbial communities. Nat. Commun. *11*, 1–13, 10.1038/s41467-020-16224-6.

Becker, N., Kunath, J., Loh, G., and Blaut, M. (2011). Human intestinal microbiota: Characterization of a simplified and stable gnotobiotic rat model. Gut Microbes *2*, 25–33, 10.4161/gmic.2.1.14651.

Belenguer, A., Holtrop, G., Duncan, S.H., Anderson, S.E., Calder, A.G., Flint, H.J., and Lobley,

G.E. (2011). Rates of productionand utilization of lactate by microbial communities fromthe human colon. FEMS Microbiol. Ecol. *77*, 107–119, 10.1111/j.1574-6941.2011.01086.x.

Brugiroux, S., Beutler, M., Pfann, C., Garzetti, D., Ruscheweyh, H.J., Ring, D., Diehl, M., Herp, S., Lotscher, Y., Hussain, S., et al. (2016). Genome-guided design of a defined mouse microbiota that confers colonization resistance against Salmonella enterica serovar Typhimurium. Nat Microbiol *2*, 16215, 10.1038/nmicrobiol.2016.215.

Butler, A.A., and Kozak, L.P. (2010). A recurring problem with the analysis of energy expenditure in genetic models expressing lean and obese phenotypes. Diabetes *59*, 323–329, 10.2337/db09-1471.

Caesar, R., Tremaroli, V., Kovatcheva-Datchary, P., Cani, P.D., and Bäckhed, F. (2015). Crosstalk between Gut Microbiota and Dietary Lipids Aggravates WAT Inflammation through TLR Signaling. Cell Metab. *22*, 658–668, 10.1016/J.CMET.2015.07.026.

Cai, T.Q., Ren, N., Jin, L., Cheng, K., Kash, S., Chen, R., Wright, S.D., Taggart, A.K.P., and Waters, M.G. (2008). Role of GPR81 in lactate-mediated reduction of adipose lipolysis. Biochem. Biophys. Res. Commun. *377*, 987–991, 10.1016/j.bbrc.2008.10.088.

Cani, P.D., Van Hul, M., Lefort, C., Depommier, C., Rastelli, M., and Everard, A. (2019). Microbial regulation of organismal energy homeostasis. Nat. Metab. *1*, 34–46, 10.1038/s42255-018-0017-4.

Chong, J., and Xia, J. (2018). MetaboAnalystR: an R package for flexible and reproducible analysis of metabolomics data. Bioinformatics *34*, 4313–4314, 10.1093/bioinformatics/bty528.

Claus, S.P., Tsang, T.M., Wang, Y., Cloarec, O., Skordi, E., Martin, F.-P., Rezzi, S., Ross, A.,

Kochhar, S., Holmes, E., et al. (2008). Systemic multicompartmental effects of the gut microbiome on mouse metabolic phenotypes. Mol. Syst. Biol. *4*, 219, 10.1038/msb.2008.56.

Corrigan, J.K., Ramachandran, D., He, Y., Palmer, C.J., Jurczak, M.J., Chen, R., Li, B., Friedline, R.H., Kim, J.K., Ramsey, J.J., et al. (2020). A big-data approach to understanding metabolic rate and response to obesity in laboratory mice. Elife *9*, 10.7554/elife.53560.

Dennis, P.P., and Bremer, H. (2008). Modulation of Chemical Composition and Other Parameters of the Cell at Different Exponential Growth Rates. EcoSal Plus *3*, 10.1128/ecosal.5.2.3.

Doi, R., Oishi, K., and Ishida, N. (2010). CLOCK regulates circadian rhythms of hepatic glycogen synthesis through transcriptional activation of Gys2. J. Biol. Chem. *285*, 22114–22121, 10.1074/jbc.M110.110361.

Duncan, S.H., Louis, P., and Flint, H.J. (2004). Lactate-utilizing bacteria, isolated from human feces, that produce butyrate as a major fermentation product. Appl. Environ. Microbiol. *70*, 5810–5817, 10.1128/AEM.70.10.5810-5817.2004.

Eberl, C., Ring, D., Münch, P.C., Beutler, M., Basic, M., Slack, E.C., Schwarzer, M., Srutkova, D., Lange, A., Frick, J.S., et al. (2020). Reproducible Colonization of Germ-Free Mice With the Oligo-Mouse-Microbiota in Different Animal Facilities. Front. Microbiol. *10*, 2999, 10.3389/fmicb.2019.02999.

Faith, J.J., Ahern, P.P., Ridaura, V.K., Cheng, J., and Gordon, J.I. (2014). Identifying gut microbe-host phenotype relationships using combinatorial communities in gnotobiotic mice. Sci. Transl. Med. *6*, 220ra11-220ra11, 10.1126/scitranslmed.3008051.

Fernández-Verdejo, R., Ravussin, E., Speakman, J.R., and Galgani, J.E. (2019). Progress and challenges in analyzing rodent energy expenditure. Nat. Methods *16*, 797–799, 10.1038/s41592-019-0513-9.

Fetissov, S.O. (2017). Role of the gut microbiota in host appetite control: Bacterial growth to animal feeding behaviour. Nat. Rev. Endocrinol. *13*, 11–25, 10.1038/nrendo.2016.150.

Fleissner, C.K., Huebel, N., El-Bary, M.M.A., Loh, G., Klaus, S., and Blaut, M. (2010). Absence of intestinal microbiota does not protect mice from diet-induced obesity. Br. J. Nutr. *104*, 919–929, 10.1017/S0007114510001303.

Flint, H.J., Duncan, S.H., Scott, K.P., and Louis, P. (2015). Links between diet, gut microbiota composition and gut metabolism. Proc. Nutr. Soc. *74*, 13–22, 10.1017/S0029665114001463.

Gordon, H.A., and Pesti, L. (1971). The gnotobiotic animal as a tool in the study of host microbial relationships. Bact. Rev. *35*, 390–429, 10.1126/science.173.3992.171.

Goswami, C., Iwasaki, Y., and Yada, T. (2018). Short-chain fatty acids suppress food intake by activating vagal afferent neurons. J. Nutr. Biochem. *57*, 130–135, 10.1016/j.jnutbio.2018.03.009.

Halatchev, I.G., O'Donnell, D., Hibberd, M.C., and Gordon, J.I. (2019). Applying indirect open-circuit calorimetry to study energy expenditure in gnotobiotic mice harboring different human gut microbial communities. Microbiome *7*, 158, 10.1186/s40168-019-0769-4.

Harley, I.T.W., and Karp, C.L. (2012). Obesity and the gut microbiome: Striving for causality. Mol. Metab. *1*, 21–31, 10.1016/j.molmet.2012.07.002.

Ishikawa, K., and Shimazu, T. (1976). Daily rhythms of glycogen synthetase and phosphorylase

activities in rat liver: influence of food and light. Life Sci. *19*, 1873–1878, 10.1016/0024-3205(76)90119-3.

Kaiyala, K.J., and Schwartz, M.W. (2011). Toward a more complete (and less controversial) understanding of energy expenditure and its role in obesity pathogenesis. Diabetes *60*, 17–23, 10.2337/db10-0909.

Koh, A., and Bäckhed, F. (2020). From Association to Causality: the Role of the Gut Microbiota and Its Functional Products on Host Metabolism. Mol. Cell *78*, 584–596, 10.1016/j.molcel.2020.03.005.

Kovatcheva-Datchary, P., Shoaie, S., Lee, S., Wahlström, A., Nookaew, I., Hallen, A., Perkins, R., Nielsen, J., and Bäckhed, F. (2019). Simplified Intestinal Microbiota to Study Microbe-Diet-Host Interactions in a Mouse Model. Cell Rep. *26*, 3772-3783.e6, 10.1016/j.celrep.2019.02.090.

Krisko, T.I., Nicholls, H.T., Bare, C.J., Holman, C.D., Putzel, G.G., Jansen, R.S., Sun, N., Rhee, K.Y., Banks, A.S., and Cohen, D.E. (2020). Dissociation of Adaptive Thermogenesis from Glucose Homeostasis in Microbiome-Deficient Mice. Cell Metab. *31*, 592-604.e9, 10.1016/J.CMET.2020.01.012.

Kuang, Z., Wang, Y., Li, Y., Ye, C., Ruhn, K.A., Behrendt, C.L., Olson, E.N., and Hooper, L. V. (2019). The intestinal microbiota programs diurnal rhythms in host metabolism through histone deacetylase 3. Science *365*, 1428–1434, 10.1126/science.aaw3134.

Kübeck, R., Bonet-Ripoll, C., Hoffmann, C., Walker, A., Müller, V.M., Schüppel, V.L., Lagkouvardos, I., Scholz, B., Engel, K.-H., Daniel, H., et al. (2016). Dietary fat and gut microbiota interactions determine diet-induced obesity in mice. Mol. Metab. *5*, 1162–1174, 10.1016/j.molmet.2016.10.001.

Levenson, S.M. (1978). The influence of the indigenous microflora on mammalian metabolism and nutrition. JPEN. J. Parenter. Enteral Nutr. *2*, 78–107, 10.1177/014860717800200203.

Levenson, S.M., Doft, F., Lev, M., and Kan, D. (1969). Influence of microorganisms on oxygen consumption, carbon dioxide production and colonic temperature of rats. J. Nutr. *97*, 542–552, 10.1093/jn/97.4.542.

Li, B., Li, L., Li, M., Lam, S.M., Wang, G., Wu, Y., Zhang, H., Niu, C., Zhang, X., Liu, X., et al. (2019). Microbiota Depletion Impairs Thermogenesis of Brown Adipose Tissue and Browning of White Adipose Tissue. Cell Rep. *26*, 2720-2737.e5, 10.1016/j.celrep.2019.02.015.

Li, M., Li, L., Li, B., Hambly, C., Wang, G., Wu, Y., Jin, Z., Wang, A., Niu, C., Wolfrum, C., et al. (2021). Brown adipose tissue is the key depot for glucose clearance in microbiota depleted mice. Nat. Commun. *12*, 1–13, 10.1038/s41467-021-24659-8.

Liebisch, G., Ecker, J., Roth, S., Schweizer, S., Öttl, V., Schött, H.F., Yoon, H., Haller, D., Holler, E., Burkhardt, R., et al. (2019). Quantification of fecal short chain fatty acids by liquid chromatography tandem mass spectrometry—investigation of pre-analytic stability. Biomolecules *9*, 121, 10.3390/biom9040121.

Lin, H. V., Frassetto, A., Kowalik Jr, E.J., Nawrocki, A.R., Lu, M.M., Kosinski, J.R., Hubert, J.A., Szeto, D., Yao, X., Forrest, G., et al. (2012). Butyrate and Propionate Protect against Diet-Induced Obesity and Regulate Gut Hormones via Free Fatty Acid Receptor 3-Independent Mechanisms. PLoS One *7*, e35240, 10.1371/journal.pone.0035240.

Liu, C., Wu, J., Zhu, J., Kuei, C., Yu, J., Shelton, J., Sutton, S.W., Li, X., Su, J.Y., Mirzadegan, T., et al. (2009). Lactate inhibits lipolysis in fat cells through activation of an orphan G-protein-coupled receptor, GPR81. J. Biol. Chem. *284*, 2811–2822, 10.1074/jbc.M806409200.

MacLean, P.S., Blundell, J.E., Mennella, J.A., and Batterham, R.L. (2017). Biological control of appetite: A daunting complexity. Obesity *25*, S8–S16, 10.1002/oby.21771.

Mallapaty, S. (2017). Gnotobiotics: getting a grip on the microbiome boom. Lab Anim. (NY). *46*, 373–377, 10.1038/laban.1344.

Mardinoglu, A., Shoaie, S., Bergentall, M., Ghaffari, P., Zhang, C., Larsson, E., Bäckhed, F., and Nielsen, J. (2015). The gut microbiota modulates host amino acid and glutathione metabolism in mice. Mol. Syst. Biol. *11*, 834, 10.15252/MSB.20156487.

Meyer, C.W., Reitmeir, P., and Tschop, M.H. (2015). Exploration of Energy Metabolism in the Mouse Using Indirect Calorimetry: Measurement of Daily Energy Expenditure (DEE) and Basal Metabolic Rate (BMR). Curr Protoc Mouse Biol *5*, 205–222, 10.1002/9780470942390.mo140216.

Mina, A.I., LeClair, R.A., LeClair, K.B., Cohen, D.E., Lantier, L., and Banks, A.S. (2018). CalR: A Web-Based Analysis Tool for Indirect Calorimetry Experiments. Cell Metab. *28*, 656–666, 10.1016/j.cmet.2018.06.019.

Moor, K., Fadlallah, J., Toska, A., Sterlin, D., Balmer, M.L., Macpherson, A.J., Gorochov, G., Larsen, M., and Slack, E. (2016). Analysis of bacterial-surface-specific antibodies in body fluids using bacterial flow cytometry. Nat Protoc *11*, 1531–1553, 10.1038/nprot.2016.091.

Murtagh, F., and Legendre, P. (2014). Ward's Hierarchical Agglomerative Clustering Method: Which Algorithms Implement Ward's Criterion? J. Classif. 2014 313 *31*, 274–295, 10.1007/S00357-014-9161-Z.

Nowak, N. (2021). Metabolic Insights Related to Sleep and Circadian Clocks from Mass

Spectrometry-Based Analysis of Blood and Breath. 10.3929/ETHZ-B-000480810.

Packard, G.C., and Boardman, T.J. (1999). The use of percentages and size-specific indices to normalize physiological data for variation in body size: Wasted time, wasted effort? Comp. Biochem. Physiol. - A Mol. Integr. Physiol. *122*, 37–44, 10.1016/S1095-6433(98)10170-8.

Popovic, M. (2019). Thermodynamic properties of microorganisms: determination and analysis of enthalpy, entropy, and Gibbs free energy of biomass, cells and colonies of 32 microorganism species. Heliyon *5*, e01950, 10.1016/j.heliyon.2019.e01950.

Rabasa, C., and Dickson, S.L. (2016). Impact of stress on metabolism and energy balance. Curr. Opin. Behav. Sci. *9*, 71–77, 10.1016/J.COBEHA.2016.01.011.

Ridaura, V.K., Faith, J.J., Rey, F.E., Cheng, J., Duncan, A.E., Kau, A.L., Griffin, N.W., Lombard, V., Henrissat, B., Bain, J.R., et al. (2013). Gut microbiota from twins discordant for obesity modulate metabolism in mice. Science *341*, 1241214, 10.1126/science.1241214.

Sayin, S.I., Wahlström, A., Felin, J., Jäntti, S., Marschall, H.U., Bamberg, K., Angelin, B., Hyötyläinen, T., Orešič, M., and Bäckhed, F. (2013). Gut microbiota regulates bile acid metabolism by reducing the levels of tauro-beta-muricholic acid, a naturally occurring FXR antagonist. Cell Metab. *17*, 225–235, 10.1016/j.cmet.2013.01.003.

Schmidt, T.S.B., Raes, J., and Bork, P. (2018). The Human Gut Microbiome: From Association to Modulation. Cell *172*, 1198–1215, 10.1016/j.cell.2018.02.044.

von Schwartzenberg, R.J., Bisanz, J.E., Lyalina, S., Spanogiannopoulos, P., Ang, Q.Y., Cai, J., Dickmann, S., Friedrich, M., Liu, S.-Y., Collins, S.L., et al. (2021). Caloric restriction disrupts the microbiota and colonization resistance. Nature 1–6, 10.1038/s41586-021-03663-4.

Smith, C.A., Want, E.J., O'Maille, G., Abagyan, R., and Siuzdak, G. (2006). XCMS: processing mass spectrometry data for metabolite profiling using nonlinear peak alignment, matching, and identification. Anal. Chem. *78*, 779–787, 10.1021/ac051437y.

Sonnenburg, J.L., and Bäckhed, F. (2016). Diet-microbiota interactions as moderators of human metabolism. Nature *535*, 56–64, 10.1038/nature18846.

Speakman, J.R. (2013). Measuring energy metabolism in the mouse - theoretical, practical, and analytical considerations. Front Physiol *4*, 34, 10.3389/fphys.2013.00034.

Steimle, A., De Sciscio, A., Neumann, M., Grant, E.T., Pereira, G. V., Ohno, H., Martens, E.C., and Desai, M.S. (2021). Constructing a gnotobiotic mouse model with a synthetic human gut microbiome to study host–microbe cross talk. STAR Protoc. *2*, 100607, 10.1016/J.XPRO.2021.100607.

Streidl, T., Karkossa, I., Segura Muñoz, R.R., Eberl, C., Zaufel, A., Plagge, J., Schmaltz, R., Schubert, K., Basic, M., Schneider, K.M., et al. (2021). The gut bacterium Extibacter muris produces secondary bile acids and influences liver physiology in gnotobiotic mice. Gut Microbes *13*, 1–21, 10.1080/19490976.2020.1854008.

Stubbs, R.J., Hopkins, M., Finlayson, G.S., Duarte, C., Gibbons, C., and Blundell, J.E. (2018). Potential effects of fat mass and fat-free mass on energy intake in different states of energy balance. Eur. J. Clin. Nutr. *72*, 698–709, 10.1038/s41430-018-0146-6.

Suárez-Zamorano, N., Fabbiano, S., Chevalier, C., Stojanović, O., Colin, D.J., Stevanović, A., Veyrat-Durebex, C., Tarallo, V., Rigo, D., Germain, S., et al. (2015). Microbiota depletion promotes browning of white adipose tissue and reduces obesity. Nat. Med. *21*, 1497–1501, 10.1038/nm.3994.

Tahara, Y., Yamazaki, M., Sukigara, H., Motohashi, H., Sasaki, H., Miyakawa, H., Haraguchi, A., Ikeda, Y., Fukuda, S., and Shibata, S. (2018). Gut Microbiota-Derived Short Chain Fatty Acids Induce Circadian Clock Entrainment in Mouse Peripheral Tissue. Sci. Rep. *8*, 1395, 10.1038/s41598-018-19836-7.

Tanner, J.M. (1949). Fallacy of per-weight and per-surface area standards, and their relation to spurious correlation. J. Appl. Physiol. *2*, 1–15, 10.1152/jappl.1949.2.1.1.

Thaiss, C.A., Zeevi, D., Levy, M., Zilberman-Schapira, G., Suez, J., Tengeler, A.C., Abramson, L., Katz, M.N., Korem, T., Zmora, N., et al. (2014). Transkingdom control of microbiota diurnal oscillations promotes metabolic homeostasis. Cell *159*, 514–529, 10.1016/j.cell.2014.09.048.

Thaiss, C.A., Levy, M., Korem, T., Dohnalova, L., Shapiro, H., Jaitin, D.A., David, E., Winter, D.R., Gury-BenAri, M., Tatirovsky, E., et al. (2016). Microbiota Diurnal Rhythmicity Programs Host Transcriptome Oscillations. Cell *167*, 1495-1510 e12, 10.1016/j.cell.2016.11.003.

Touw, K., Ringus, D.L., Hubert, N., Wang, Y., Leone, V.A., Nadimpalli, A., Theriault, B.R., Huang, Y.E., Tune, J.D., Herring, P.B., et al. (2017). Mutual reinforcement of pathophysiological host-microbe interactions in intestinal stasis models. Physiol. Rep. *5*, e13182, 10.14814/PHY2.13182.

Tschop, M.H., Speakman, J.R., Arch, J.R., Auwerx, J., Bruning, J.C., Chan, L., Eckel, R.H., Farese Jr., R. V, Galgani, J.E., Hambly, C., et al. (2011). A guide to analysis of mouse energy metabolism. Nat Methods *9*, 57–63, 10.1038/nmeth.1806.

Turnbaugh, P.J., Ley, R.E., Mahowald, M.A., Magrini, V., Mardis, E.R., and Gordon, J.I. (2006). An obesity-associated gut microbiome with increased capacity for energy harvest. Nature *444*, 1027–1031, 10.1038/nature05414.

Ucar, I., Pebesma, E., and Azcorra, A. (2019). Measurement errors in R. R J. *10*, 549–557, 10.32614/RJ-2018-075.

Walter, J., Armet, A.M., Finlay, B.B., and Shanahan, F. (2020). Establishing or Exaggerating Causality for the Gut Microbiome: Lessons from Human Microbiota-Associated Rodents. Cell *180*, 221–232, 10.1016/j.cell.2019.12.025.

Wang, Y., Kuang, Z., Yu, X., Ruhn, K.A., Kubo, M., and Hooper, L. V. (2017). The intestinal microbiota regulates body composition through NFIL3 and the circadian clock. Science *357*, 912–916, 10.1126/science.aan0677.

Weir, J.B.D.B. (1949). New methods for calculating metabolic rate with special reference to protein metabolism. J. Physiol. *109*, 1–9, 10.1113/jphysiol.1949.sp004363.

Weiss, A.S., Burrichter, A.G., Chakravarthy Durai Raj, A., Von, A., Meng, C., Kleigrewe, K., Münch, P.C., Rössler, L., Eisenreich, W., Jochum, L.M., et al. (2021). Exploring the interaction network of a synthetic gut bacterial community. BioRxiv 2021.02.25.432904, 10.1101/2021.02.25.432904.

White, C.R., and Seymour, R.S. (2005). Allometric scaling of mammalian metabolism. J. Exp. Biol. *208*, 1611–1619, 10.1242/jeb.01501.

Wostmann, B.S., Bruckner-Kardoss, E., and Knight, P.L. (1968). Cecal Enlargement, Cardiac Output, and O2 Consumption in Germfree Rats. Exp. Biol. Med. *128*, 137–141, 10.3181/00379727-128-32962.

Wostmann, B.S., Larkin, C., Moriarty, A., and Bruckner-Kardoss, E. (1983). Dietary intake, energy metabolism, and excretory losses of adult male germfree Wistar rats. Lab. Anim. Sci. *33*,

46–50.

Woting, A., Pfeiffer, N., Loh, G., Klaus, S., and Blaut, M. (2014). Clostridium ramosum promotes High-Fat diet-induced obesity in Gnotobiotic Mouse Models. MBio *5*, 1530–1544, 10.1128/mBio.01530-14.

Woting, A., Pfeiffer, N., Hanske, L., Loh, G., Klaus, S., and Blaut, M. (2015). Alleviation of high fat diet-induced obesity by oligofructose in gnotobiotic mice is independent of presence of Bifidobacterium longum. Mol. Nutr. Food Res. *59*, 2267–2278, 10.1002/mnfr.201500249.

Wotzka, S.Y., Kreuzer, M., Maier, L., Arnoldini, M., Nguyen, B.D., Brachmann, A.O., Berthold, D.L., Zünd, M., Hausmann, A., Bakkeren, E., et al. (2019). Escherichia coli limits Salmonella Typhimurium infections after diet shifts and fat-mediated microbiota perturbation in mice. Nat. Microbiol. 10.1038/s41564-019-0568-5.

Yao, L., Seaton, S.C., Ndousse-Fetter, S., Adhikari, A.A., DiBenedetto, N., Mina, A.I., Banks, A.S., Bry, L., and Devlin, A.S. (2018). A selective gut bacterial bile salt hydrolase alters host metabolism. Elife *7*, 10.7554/eLife.37182.

Yilmaz, B., Mooser, C., Keller, I., Li, H., Zimmermann, J., Bosshard, L., Fuhrer, T., Gomez de Agüero, M., Trigo, N.F., Tschanz-Lischer, H., et al. (2021). Long-term evolution and short-term adaptation of microbiota strains and sub-strains in mice. Cell Host Microbe *29*, 650-663.e9, 10.1016/j.chom.2021.02.001.

Zarrinpar, A., Chaix, A., Yooseph, S., and Panda, S. (2014). Diet and feeding pattern affect the diurnal dynamics of the gut microbiome. Cell Metab. *20*, 1006–1017, 10.1016/j.cmet.2014.11.008.

Zarrinpar, A., Chaix, A., Xu, Z.Z., Chang, M.W., Marotz, C.A., Saghatelian, A., Knight, R., and Panda, S. (2018). Antibiotic-induced microbiome depletion alters metabolic homeostasis by affecting gut signaling and colonic metabolism. Nat. Commun. 2018 91 *9*, 1–13, 10.1038/s41467-018-05336-9.

SUPPLEMENTARY TABLE

Supplementary Table 1. List of metabolites identified by targeted peak extraction in the UPLC/MS data. Table indicates compound name, KEGG Entry number, type of column was used for UPLC and if the peak ID matched the retention time and MS2 spectra identified with the chemical standard in liver and plasma samples.

Compound	**KEGG Entry**	**Column**	**Matched peak ID in Liver**	**Matched peak ID in Plasma**
(R)-3-hydroxybutanic acid	C01089	RP Negative	Yes	No
5-Oxoproline	C01879	AMIDE Positive	Yes	Yes
Arachidonic acid	C00219	RP Negative	Yes	Yes
Betaine	C00719	AMIDE Positive	No	Yes
beta-Murocholic acid	C17726	RP Negative	Yes	Yes
Cholic acid	C00695	RP Negative	Yes	Yes
Citrulline	C00327	AMIDE Positive	Yes	Yes
Cortisol	C00735	RP Positive	Yes	No
Creatine	C00300	AMIDE Positive	Yes	Yes

Creatinine	C00791	AMIDE Positive	No	Yes
Cystathionine	C02291	AMIDE Positive	Yes	Yes
Deoxycholic acid	C04483	RP Negative	No	Yes
Docosapentaenoic acid	C16513	RP Negative	Yes	Yes
Glutathione (GSH)	C00051	AMIDE Positive	No	Yes
Glycine	C00037	AMIDE Positive	Yes	Yes
Glycocholic acid	C01921	RP Positive	Yes	No
Hexadecanedioic acid		RP Negative	Yes	Yes
Hippuric acid	C01586	RP Negative	Yes	Yes
L-(+)-Ornithine	C00077	AMIDE Positive	Yes	Yes
L-4-Hydroxyproline	C01157	AMIDE Positive	Yes	Yes
L-Alanine	C00041	AMIDE Positive	Yes	Yes
L-Arginine	C00062	AMIDE Positive	Yes	Yes
Lauroylcarnitine		RP Positive	Yes	Yes

Leucine	C00123	RP Positive	Yes	Yes
L-Glutamic acid	C00025	AMIDE Positive	Yes	Yes
L-Histidine	C00135	AMIDE Positive	Yes	Yes
Linoleic acid	C01595	RP Negative	Yes	Yes
L-Isoleucine	C00407	RP Positive	Yes	Yes
L-Lysine	C00047	AMIDE Positive	Yes	Yes
L-Methionine	C00073	AMIDE Positive	Yes	Yes
L-Proline	C00148	AMIDE Positive	Yes	Yes
L-Serine	C00065	AMIDE Positive	Yes	Yes
L-Threonine	C00188	AMIDE Positive	Yes	Yes
L-Tryptophan	C00078	RP Negative	Yes	Yes
L-Tyrosine	C00082	RP Negative	Yes	Yes
Myristic acid	C06424	RP Negative	Yes	Yes
N,N-dimethylglycine	C01026	AMIDE Positive	Yes	Yes

N-Acetylmethionine	C02712	RP Positive/Negative	Yes	Yes
Oxidized glutathione (GSSG)	C00127	AMIDE Negative	Yes	Yes
Pantothenic acid	C00864	RP Positive	Yes	Yes
Pipecolinic acid	C00408	RP Positive	Yes	Yes
Serotonin	C00780	RP Positive	Yes	Yes
Succinic acid	C00042	RP Negative	Yes	Yes
Taurine	C00245	AMIDE Negative	Yes	Yes
Taurine-beta-murocholic acid		AMIDE Negative	Yes	Yes
Taurochenodeoxycholic acid	C05465	AMIDE Negative	Yes	Yes
Tetradecanedioic acid		RP Negative	Yes	Yes

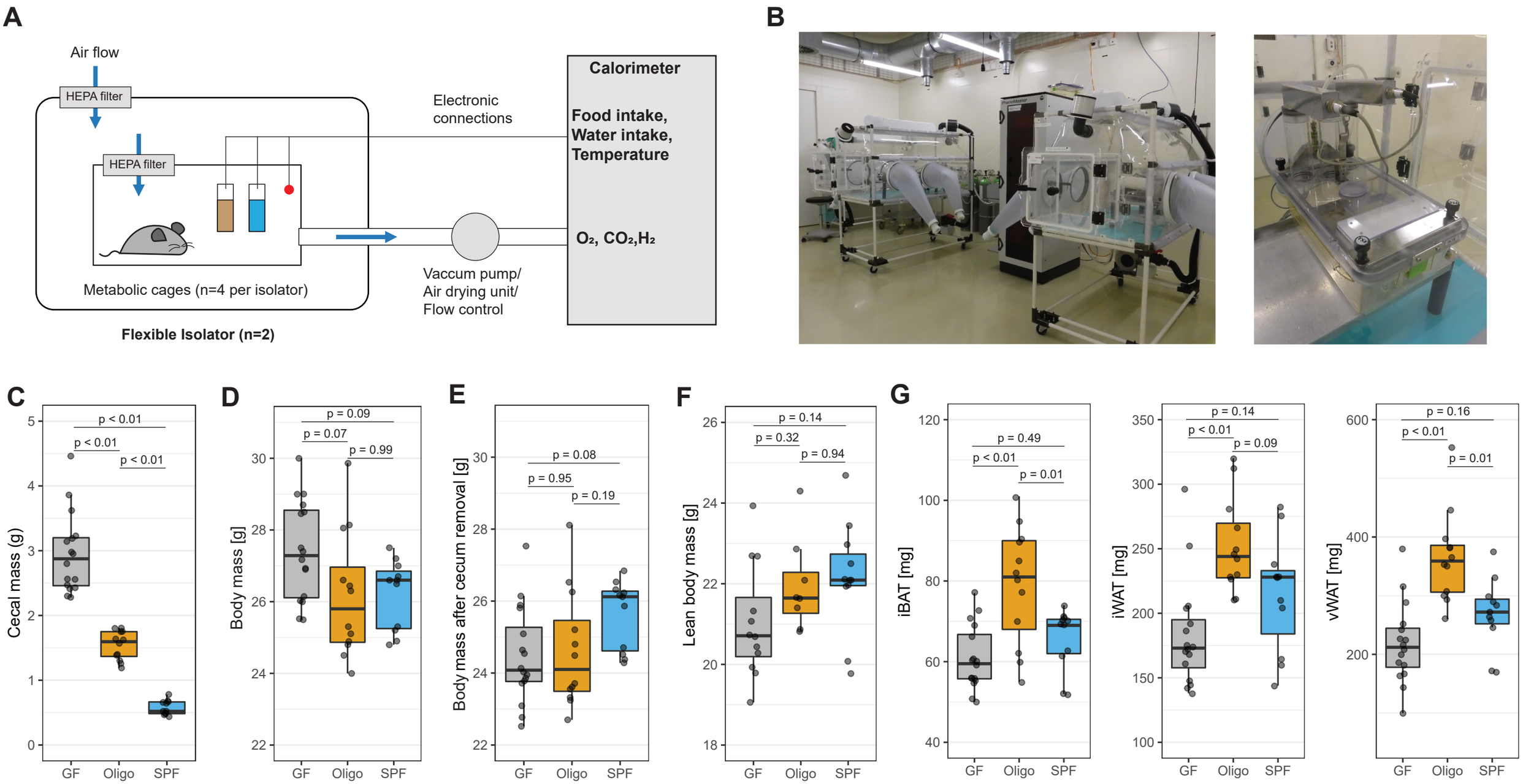

Figure 1: OligoMM12 mice have increase fat mass compared to GF mice and SPF C57B6/J mice.

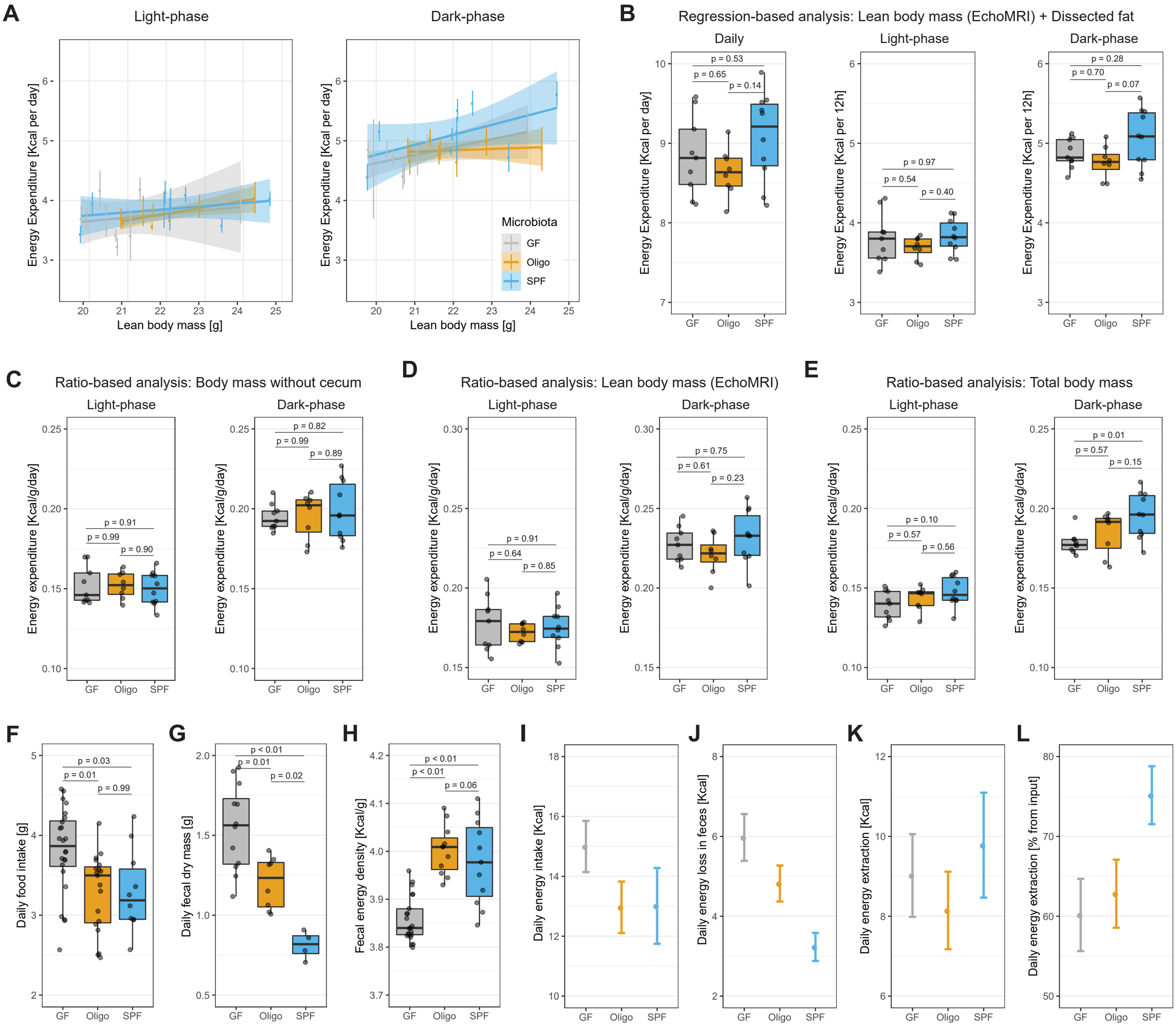

Figure 2: Energy metabolism in GF, OligoMM12 and SPF C57B6/J mice.

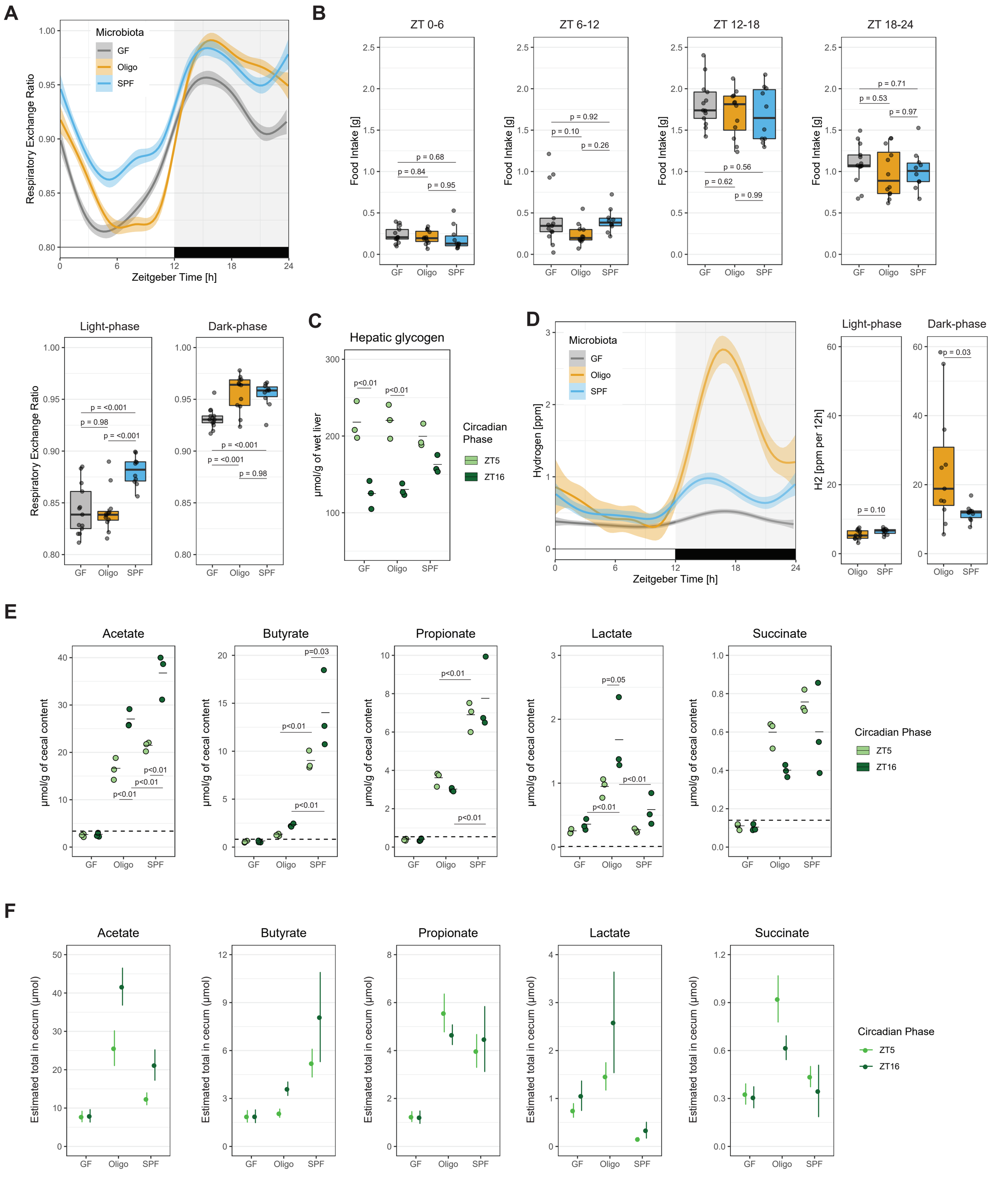

Figure 3: Circadian changes in Respiratory Exchange Ratio (RER), microbiota-derived hydrogen and short-chain fatty acids (SCFAs).

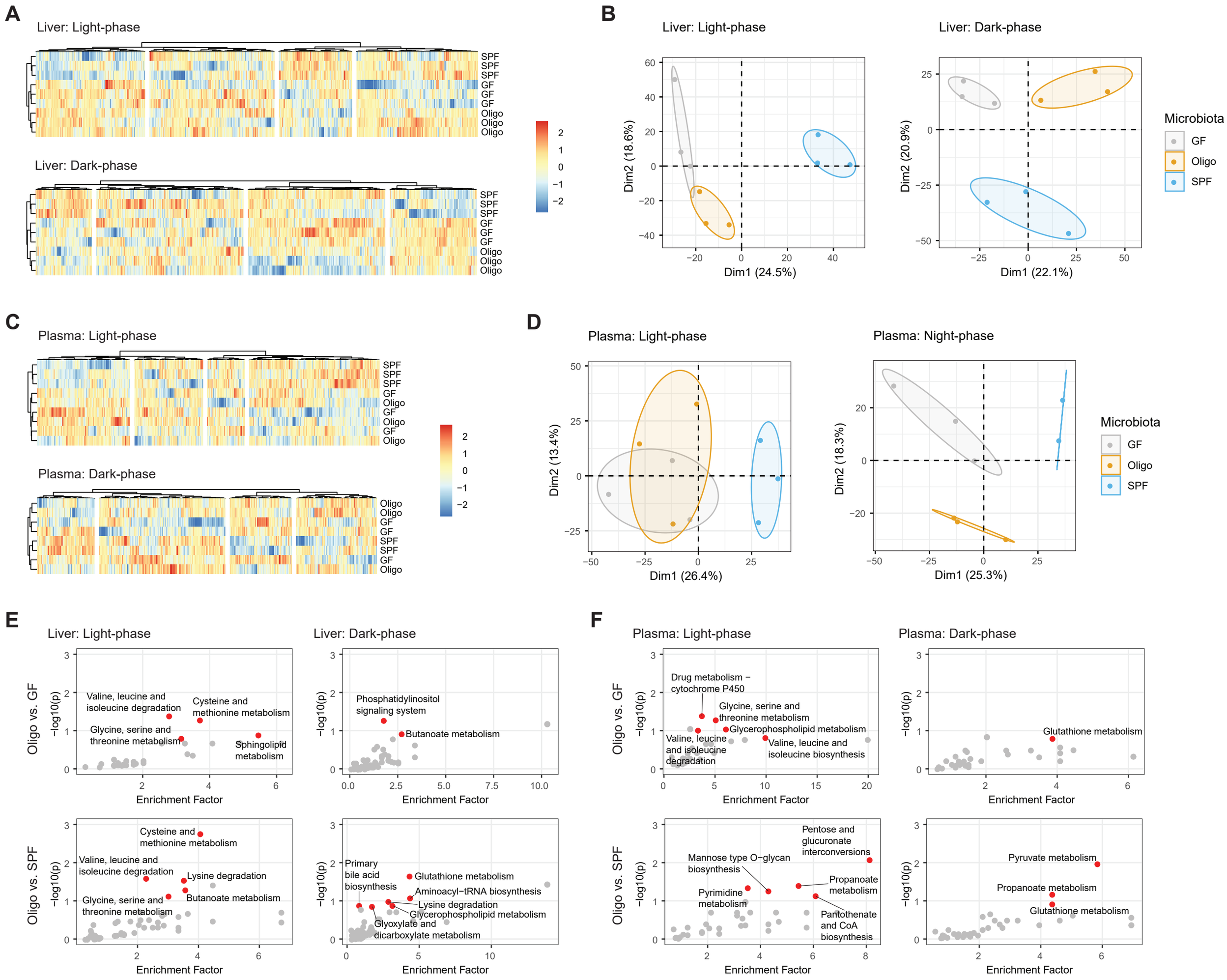

Figure 4. Metabolic profile comparison of GF, OligoMM12 and SPF mice by UPLC/MS.

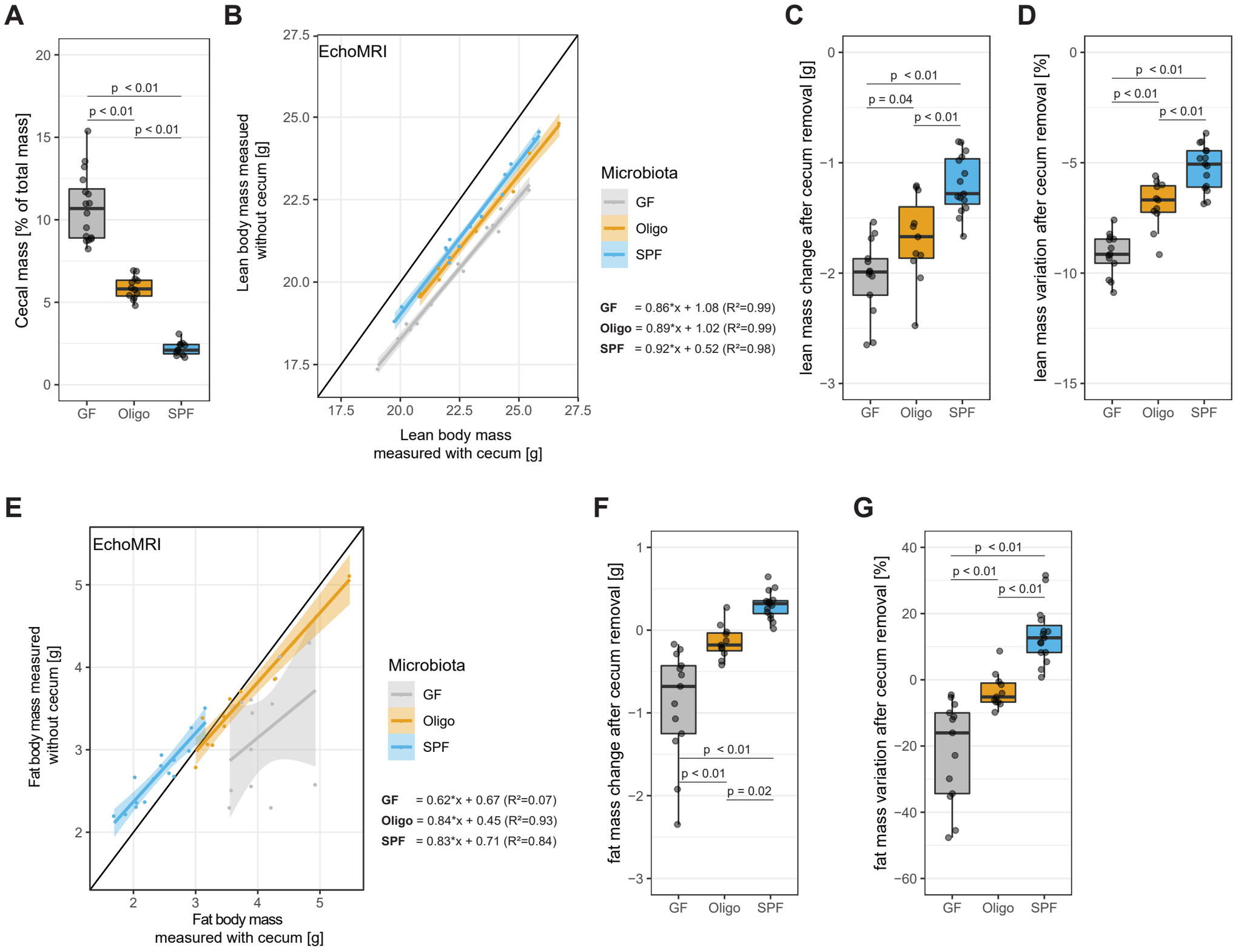

Supplementary Figure 1: Cecal mass interferes with fat mass estimation by Echo-MRI.

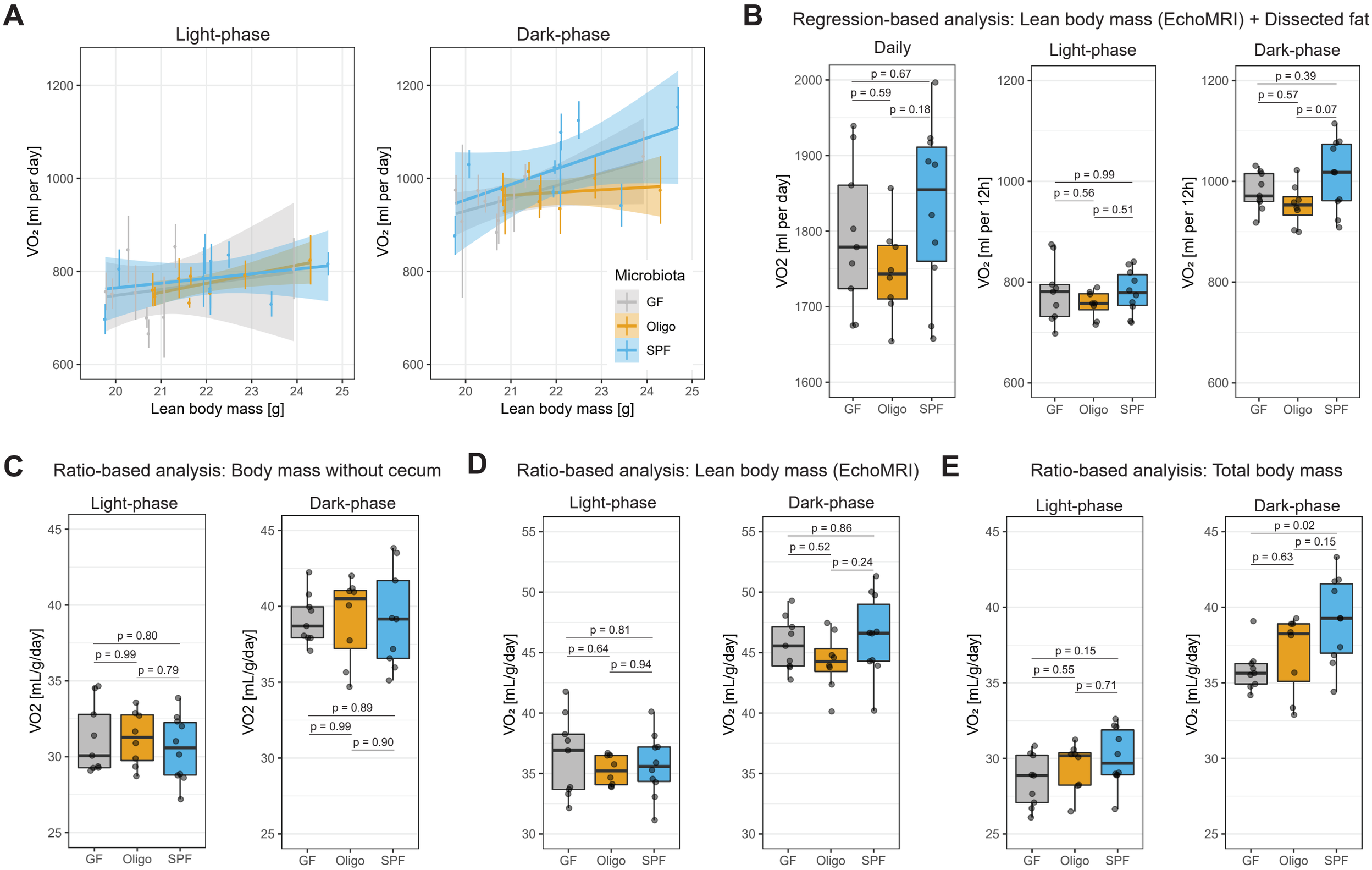

Supplementary Figure 2: Cecal mass interferes with normalization of VO2 and Energy Expenditure.

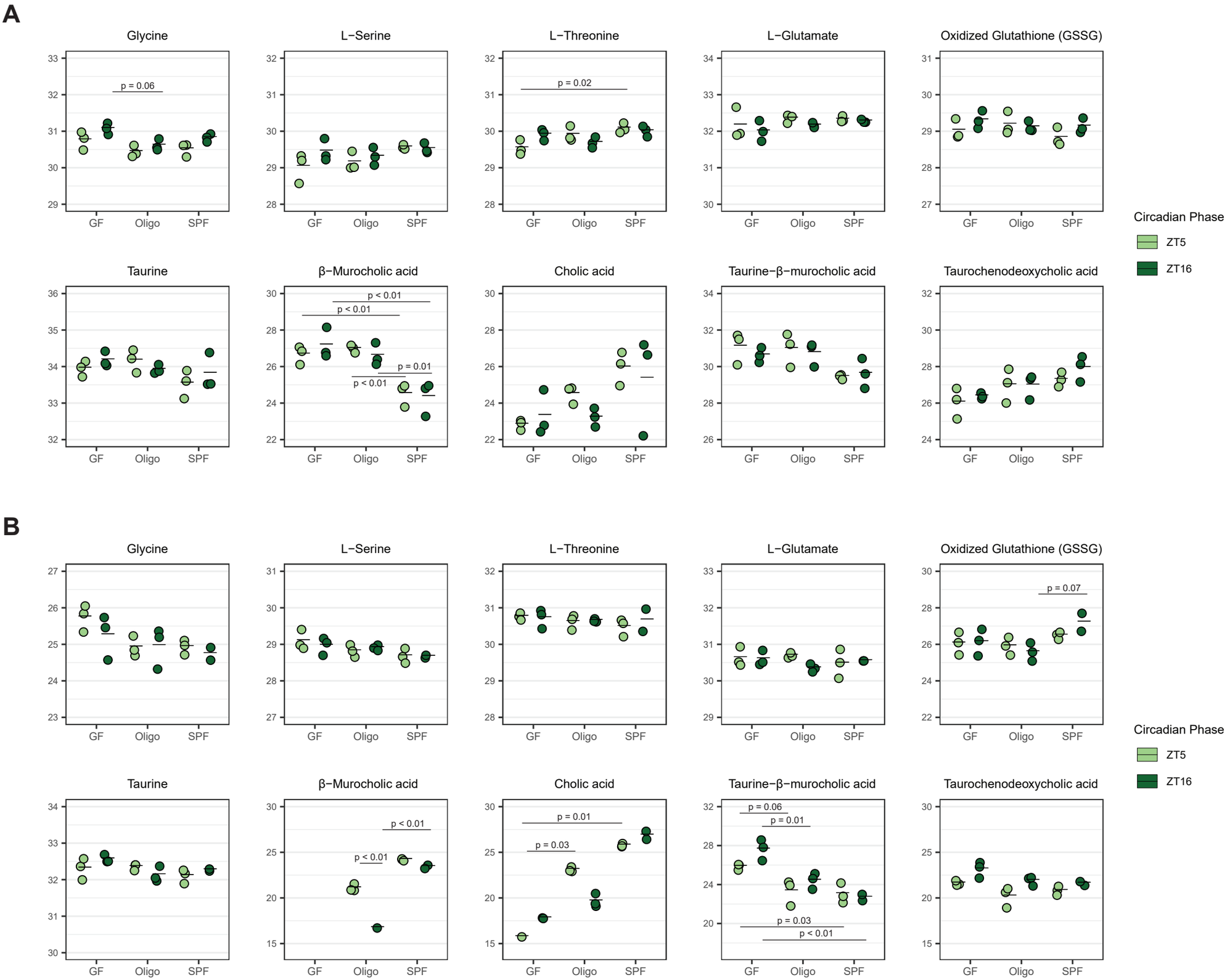

Supplementary Figure 3. Metabolic profile comparison of GF, OligoMM12 and SPF mice by UPLC/MS (targeted peak extraction of selected list of compounds)